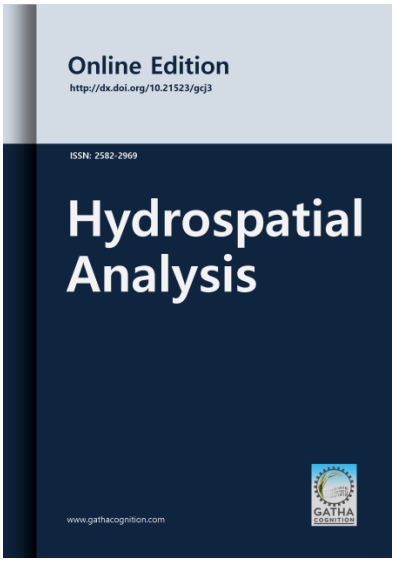

Hydrospatial Analysis

Editor-in-Chief: **Professor Pramodkumar Hire**

EISSN: 2582-2969

DOI: https://doi.org/10.21523/gcj3

Assessment of Flood Susceptibility Mapping in the Krishna River Basin using Geospatial Techniques

Vinod P. Gaikwad[1*], Sanjay B. Navale[1], Avinash B. Hande

Department of Geography, S. N. Arts, D.J. Malpani Commerce and B. N. Sarda Science College, Sangamner, Ahilyanagar, Maharashtra, India.

To cite this article

Gaikwad, V. P., Navale, S. B. and Hande, A. B., 2026. Assessment of flood susceptibility mapping in the Krishna river basin using geospatial techniques. *Hydrospatial Analysis*, 10(1), 1-24.

DOI: https://doi.org/10.21523/gcj3.2026100101

GATHA COGNITION

https://gathacognition.com

Hydrospatial Analysis
Homepage: www.gathacognition.com/journal/gcj3
http://dx.doi.org/10.21523/gcj3

Original Research Paper

Assessment of Flood Susceptibility Mapping in the Krishna River Basin using Geospatial Techniques

Vinod P. Gaikwad[1*], Sanjay B. Navale[1], Avinash B. Hande

Department of Geography, S. N. Arts, D. J. Malpani Commerce and B. N. Sarda Science College, Sangamner, Ahilyanagar, Maharashtra, India.

Abstract

A flood is an excess of water that swamps normally dry land due to heavy rainfall, storm surges, or dam failures, often leading to significant damage and displacement. This study evaluates flood susceptibility in Krishna River Basin (KRB) (India) using geospatial techniques and the Analytical Hierarchy Process (AHP). Thirteen physiographic parameters elevation, slope, proximity to rivers, geomorphology, drainage density, flow accumulation, rainfall, land use/land cover (LULC), geology, soil type, Stream Power Index (SPI), Topographic Wetness Index (TWI), and curvature were integrated into a multi-criteria decision framework and processed in ArcGIS 10.8. Pairwise comparison matrices assigned weights to parameters, validated by a consistency ratio (CR = 0.04), ensuring robust model reliability.

The results classify the KRB into five susceptibility zones: very low (21%), low (21%), moderate (20%), high (19%), and very high (19%). High-risk areas correlate with low-lying floodplains, clay-loam soils, dense drainage networks, and built-up-agricultural zones. The validation of the Analytical Hierarchy Process (AHP) using the Area Under the Curve (AUC) indicated robust performance, achieving 79% accuracy. Approximately 30 cities, including Pune, Vijayawada, and Solapur, face significant flood threats. The present study offers actionable intelligence for providing a spatial decision-support framework for prioritizing flood mitigation investments, enforcing land-use zoning in high-risk zones, and optimizing reservoir operations to manage downstream flood peaks. This research underscores the value of geospatial-AHP integration, offering actionable insights for urban planners and disaster management authorities to enhance community resilience. Future research should integrate real-time data and machine learning for dynamic predictions while considering local human impacts.

Article History

Received: 26 September 2025
Revised: 15 November 2025
Accepted: 20 November 2025
Published: 05 March 2026

Keywords

Geospatial Techniques;
Flood Susceptibility;
Analytical Hierarchy Process;
Krishna River Basin;
GIS.

Editor(s)

P. Hire
Vijay Bhagat

1 INTRODUCTION

Floods are a natural part of the water cycle (Vojtek and Vojtekova, 2016) mainly caused by snowmelt, sudden cloudbursts, and heavy rainfall in semi-arid regions or wind-driven waves in coastal and estuarine areas (Tehrany *et al*., 2013; Merkuryeva *et al*., 2015) significantly impacting human life and infrastructure (Das, 2018; Debnath *et al*., 2023; Winsemiu *et al*., 2016). The flood hazards are heightened by climatic changes, land use modifications, and human activities such as urban sprawl, stream diversion, deforestation, and excessive groundwater extraction (Kourgialas and Karatzas, 2011; Khodaei *et al*., 2025; Abijith *et al*., 2025; Kvocka *et al*., 2016). However, modern tools can be used to effectively monitor river overflow floods (Jonkman, 2005; Das, 2018).

* Author address for correspondence
Department of Geography, S. N. Arts, D.J. Malpani Commerce and B. N. Sarda Science College, Sangamner, Ahilyanagar, Maharashtra, India.
Tel.: +919689057274
Emails: gaikwadvinod549@gmail.com (*V. Gaikwad* -Corresponding author); navalesanju1979@gmail.com (*S. Navale*); avihande33@gmail.com (*A. Hande*).

https://doi.org/10.21523/gcj3.2026100101

Floods are a complex event that has been widely studied by researchers to better understand their causes and develop effective methods for control and prevention (Miguez, and Magalhaes, 2010; Wang, *et al*., 2022). In addition to natural as well as man-made factors continuous rainfall is also a major factor in flooding (Kim and Kim, 2014). Furthermore, human changes in land use in upstream areas of flood zones increase the risk and impact of flooding (Gigović *et al*., 2017). Recently, extreme flooding events have occured due to the climate change phenomenon (Rojas *et al*., 2012; Halgamuge and Nirmalathas, 2017). Fluctuations in climate patterns, such as increased precipitation, rising sea levels, and altered weather systems, have the potential to intensify flooding, thereby increasing both the regularity and rigorousness of such events. Apart from these reasons, human factors are also involved in the creation of flood situation such as, poor management, improper planning, mismanaged reservoir discharges, limited drainage capacity, monsoons, and inadequate flood mitigation measures. According to Saha and Agrawal (2020), applying specific, effective mitigation strategies can help reduce the intensity of a disaster, even though it is not possible to fully eliminate the hazards associated with flood events. Therefore, understanding the impact of climate change is crucial for accurately evaluating flood threats and formulating effective mitigation measures (Wang, *et al*., 2022; Das, 2018). Floods are a significant threat to the economy and the livelihoods of individuals, underscoring the need for the proper flood risk management to reduce the damage caused by these events.

According to Lim and Lee (2017), Flood conditions are influenced by geographic features such as the slope inclination of the land, the river course, the geology of riverbed, distance from the main channel, terrain curvature as well as the elevation and geological composition of the area. The rapid urbanization and industrialization along riverbanks, driven by population growth, disrupt the natural river flow and lead to the narrowing of river channels. In recent years, rivers worldwide have been experiencing more frequent and severe flooding events. Flooding frequently occurs across Asian countries, including China and Nepal, affecting the major rivers such as the Yangtze and Yellow in China, the Kosi and Pokhara region in Nepal (2008, 2012), along with several Indian rivers like the Ganga (2005) and Krishna (Dimri *et al*., 2016). In Maharashtra, where the Krishna River basin is originated, major rivers respond rapidly to intense monsoon rainfall, often resulting in severe flooding in low-lying and densely populated areas of Krishna (2019, 2021), Mutha (2024), and Godavari (2006, 2008, 2024). These flood events lead to the degradation of both natural and human resources.

Recent research highlights the significance of flood hazard mapping and demarcation of flood-susceptibility using deep learning and machine learning approach (Efraimidou and Spiliotis, 2024; Al-Ruzouq *et al*., 2024; Razavi-Termeh *et al*., 2025; Arora *et al*., 2025; Pourzangbar *et al*., 2025; Tepetidis *et al*., 2025; Abijith *et al*., 2025; Wale *et al*., 2025). Ekmekcioglu *et al*., (2022) emphasized the role of geospatial technologies in flood assessment. Similarly, Gupta and Dixit (2022) applied GIS-based models to evaluate flood risks, enhancing flood management strategies. Malekian and Azarnivand (2016) also used GIS and RS to assess the flood susceptible areas, demonstrating the effectiveness of spatial data in flood risk evaluation. Many studies on flood hazards have been done at different levels such as Tique *et al*., (2025) utilized remote sensing and machine learning to develop 30 m flood susceptibility maps for Nigeria, revealing that approximately 11 million people reside in high-risk flood zones. The Copernicus DEM with D8/FD8 methods gave the most accurate results of Nigeria. Dou *et al*. (2017) studied regional flood risks, while Muis *et al*. (2015) examined floods globally. Su *et al*. (2011) focused on China, studying floods and snow disasters across the country and how they affect people and places. Das *et al*. (2017, 2018) emphasized that RS and GIS are crucial tools for disaster risk management with spatial mapping using multi-criteria decision models. Diyali Chattaraj *et al*. (2021) study flood and waterlogging risks at a local level. They use an AHP and GIS model to improve hazard assessment and management. Many studies have been conducted around the world, including India, to understand flood causes and damage (Tehrany *et al*., 2013; Suykens *et al*., 2016; Risi *et al*., 2017; Marvi, 2020; Atif *et al*., 2021; Yu *et al*., 2022). Furthermore, numerous researchers have integrated GIS technique with AHP and fuzzy AHP methods to generate flood risk maps (Hammami *et al*., 2019; Meshram *et al*., 2019; Ekmekcioglu *et al*., 2021; Zhran *et al*., 2024). Islam (2024) has attempted to evaluate the flood susceptibility using bivariate statistical method. However, most of these studies focus on improving specific flood control methods for particular assets (Zhang and Alipour, 2021).

Flood risk assessment using geospatial techniques involves analyzing spatial data to identify flood-prone areas and assessing the potential impacts of flooding. The Krishna River, the third-longest river in India, originates in the Western Ghats near Mahabaleshwar, Maharashtra, at an elevation of 1300 meters. It flows eastward through *Wai* and eventually drains into the Bay of Bengal. Flooding in the Krishna River is exacerbated by inadequate river management, with Maharashtra and Karnataka filling reservoir to capacity and subsequently releasing large volume of water downstream leads to flooding in the lower reaches and backwater areas.

Geospatial techniques enable detailed mapping and analysis of terrain hydrology, land use to support effective flood management and mitigation strategies. The study assesses the factors causing floods and mapped flood-prone regions in the Krishna River Basin (KRB) applying the geospatial methods. This will help equip the residents of the region with the ability to forecast potential flood risks and promptly execute localized interventions to manage flood situations as they arise.

2 STUDY AREA

The Krishna River is the third longest in India after the Ganga and Godavari, and it forms the fourth largest river basin in the country, covering 2,58,948 km^2, which is about 8% of India's total area. It spans Maharashtra (26.36%), Karnataka (43.8%), Telangana and Andhra Pradesh (29.81%). The basin is 701km long and 672km in wide. The longitudinal extend is 73°17′ to 81°9′ E and the latitudinal extend is 13°10′ to 19°22′ N. The *Balaghat* range extends widely to the north, with the Eastern Ghats extending from to the southeast, and the Western Ghats to the west. The KRB is fed through numerous tributaries, including the *Bhima, Tungabhadra, Malaprabha, Ghataprabha, Munneru*, and others, which significantly contribute to its water flow. The altitude of the basin ranges from 600m to 2100m. The Krishna Basin, near the Western Ghat experiences torrential rainfall and high humidity, while the Deccan plains feature a tropical climate under the influence of the southwest monsoon winds which brings majority of precipitation. Around 90% of the annual rainfall in the Krishna Basin takes place throughout the monsoon season, with over 70% falling in July to September. The basin area experiences mean annual temperature around 26°C. The major soil categories in KRB contain black, red, laterite, alluvial, saline-alkaline, and mixed soils, etc. The Basin, encompassing 47 districts across four states, has a total population of 142668920. The major dams over the Krishna River include Srisailam, Nagarjuna Sagar (Andhra Pradesh and Telangana), Vanivilas Sagar, Almatti, Malaprabha, Bhadra, Hidkal (Karnataka), and Koyna, Ujjani, Radhanagari (Maharashtra), vital for water supply, irrigation, and power generation. Vijayawada, Hyderabad, Kurnool, and Guntur (Andhra Pradesh); Solapur, Kolhapur, and Sangli (Maharashtra); and Bagalkot, Belagavi, and Raichur (Karnataka) are the major cities in the KRB and all of which play vital roles in the region's economy and development (WRIS, 2018; Kumar and Jayakumar, 2020).

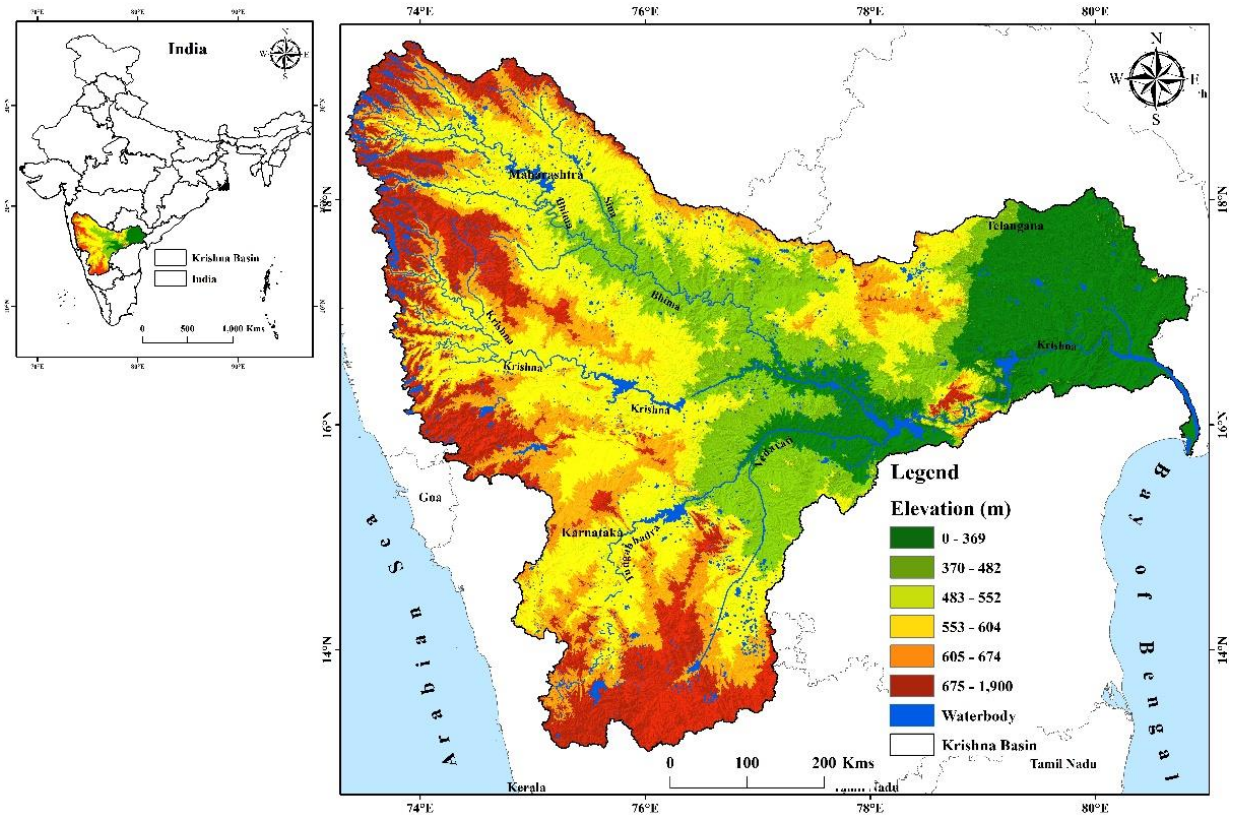

Figure 1. Study area: Krishna basin (India)

3 METHODOLOGY

The location map was generated using Shuttle Radar Topography Mission (SRTM) Digital Elevation Model (DEM) data at a 90m resolution, employing the hydrology analysis tools within the ArcMap 10.8 software environment (Figure 1). The freely available SRTM 90m DEM, with a vertical accuracy of ±16 m, has been widely validated and applied in hydrological studies (Farr *et al*., 2007; Gangani *et al*., 2023; Bielski *et al*., 2024). It remains suitable for large-scale basins such as the Krishna, providing adequate accuracy, consistency, and feasibility for regional flood assessment. Key terrain characteristics, containing elevation, slope, curvature, flow accumulation, and drainage networks, were analyzed to construct the drainage density map. River proximity was quantified using spatial buffering techniques in ArcMap. Geospatial data on geology and geomorphology were sourced from the GSI. Rainfall distribution maps were developed utilizing meteorological datasets procured from the Indian Meteorological Department, Pune. Land use and land cover (LULC) mapping was facilitated by Landsat 8-9 Enhanced Thematic Mapper Plus (ETM+) imagery, with a spatial resolution of 30 m. Soil texture information, essential for the soil texture mapping of the Krishna basin, was acquired from the National Bureau of Soil Survey and Land Use Planning (NBSS and LUP), ensuring data precision and integrity. The Topographic Wetness Index (TWI) and Stream Power Index (SPI) were derived directly within the ArcMap framework using the DEM data.

A flood susceptibility assessment has been conducted in the KRB, using a multi-criteria analysis context based on the AHP as proposed by Saaty (1980). The evaluation incorporated a comprehensive set of physiographic criteria, including Elevation, Slope, and Proximity to the river, Geomorphology, Drainage

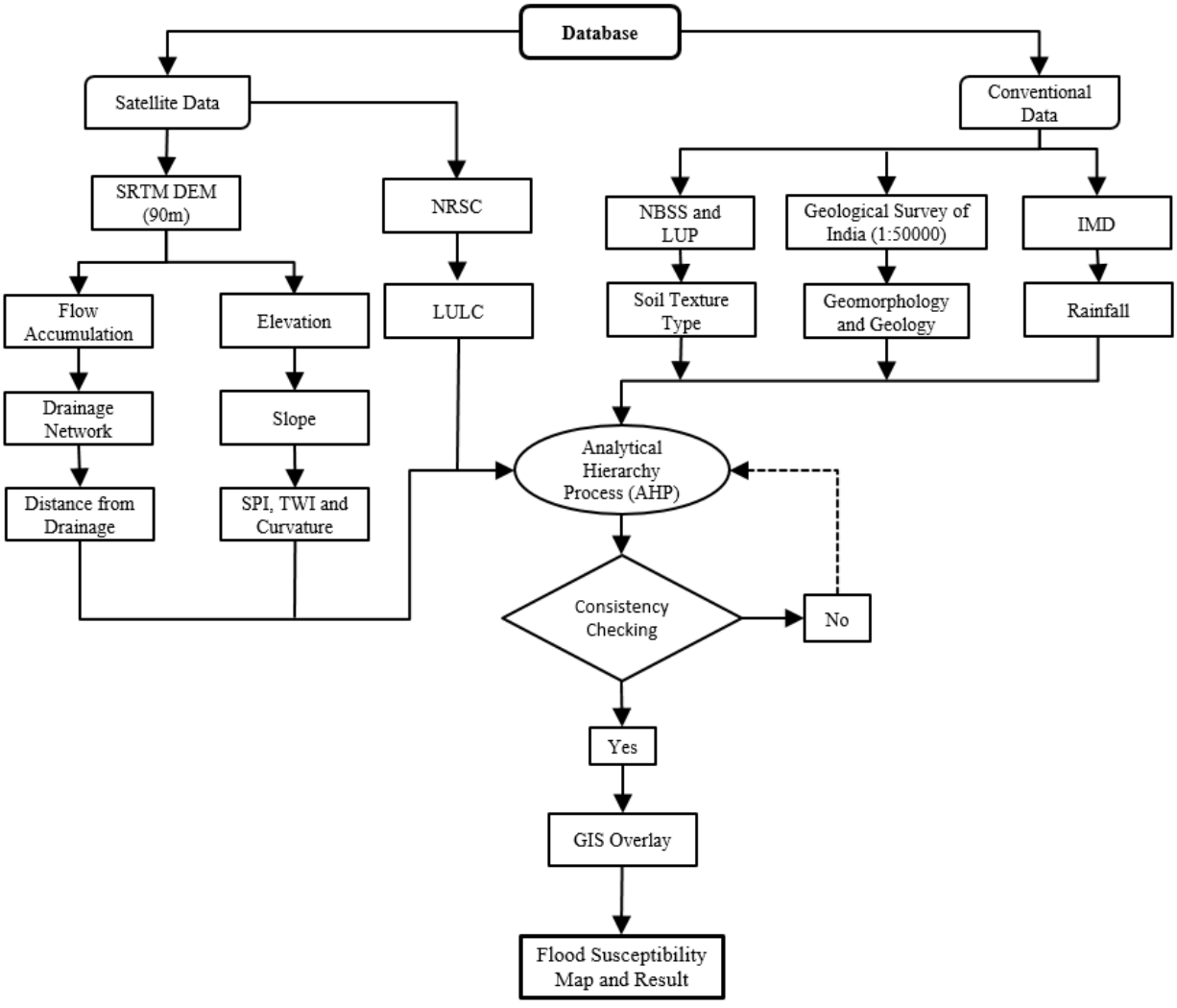

Figure 2. Methodology

density, Flow accumulation, Rainfall, LULC, Geology, Soil type, SPI, TWI, and Curvature. This technique offers a rigorous, efficient tactic for detecting flood-prone areas, thereby supporting effective water resource management and mitigation policies within the basin. The analytical procedure comprised six sequential steps: criteria selection, ranking of criteria, pairwise comparison, weight calculation, score assignment, and execution of a weighted overlay analysis. These methodological steps were pivotal in delineating areas susceptible to flooding, thereby enhancing the understanding of flood risk dynamics and informing strategic planning in the KRB.

3.1 Analytical Hierarchy Process (AHP) model

The major factors influencing flood susceptibility include elevation, slope gradient, river proximity, Rainfall, flow accumulation, LULC, geological structure, TWI, and surface curvature. To demarcate the flood prone areas in KRB multiple parameters have been taken into account on the basis of their relative significance in the decision-making method. The structured categorization, optimization of efficiency, and generation of precise outcomes are fundamental attributes of the AHP (Das, 2019; Gaikwad, 2019). The AHP is extensively applied for managing water resources. The analysis rigorously incorporated a comprehensive suite of thirteen physiographic parameters. Each criterion has gave a rank based on its significance, aiding in the organization and prioritization of spatial decisions (Saaty, 1977; Das, 2019; Navale and Bhagat, 2021). The most important criteria were assigned higher weights whereas the least important were given lower weights. The Pairwise Comparison Matrix (PWCM) in AHP assesses factors influencing flood susceptibility using Saaty's scale (1977), with values ranging from 9 to 1/9 to indicate relative significance. These comparisons help calculate priority weights for decision-making in flood prone mapping. In the present work, criteria were ranked from 1 to 9, with expert input determining the significance of each factor. AHP is an innovative and flexible method in statistics, widely used in research for analyzing multiple factors and predicting outcomes accurately to solve complex problems. The AHP method has been applied to assign weights and ranks to different parameters in the flood prone index model, as shown below:

$$FH = \sum_{i=1}^{n} Wi * Ri \qquad (1)$$

Where, *FH* is the flood hazard index, *Wi* is the weight of each factor, and *Ri* is the rank of each factor's value. The final map in this study is categorized into five classes: very low, low, moderate, high, and very high, using the FH model to assess the probability of flood occurrence (Das, 2018).

AHP calculates parameter weights using the Pairwise Comparison Matrix (PCM) based on the relative importance and influence of each factor on the basis of extensive literature review and the expert opinion. These weights establish the importance of each parameter in a hierarchical structure. After calculating the weights in PCM, the matrix is normalized by dividing respectively judgment value by the total of its column. The quotient values for each row are summed and then divided by the number of parameters in the PCM (Table 1). The resultant value for each parameter represents its weight, extending from 0 to 1, with the sum of all weights constantly equal to 1.

A PCM is established, with diagonal elements set to 1 (Eq. 2). The relative prominence of the criteria has determined based on predefined criteria, assigning ranks as follows: 1 for equally important, 3 for moderately more important, 5 for strongly more important and 7 for very strongly more important. Intermediate values, such as 2, 4, and 6, are used to represent varying degrees of importance (Dejen and Soni 2021). Each row shows how important one parameter is compared to others. For example, the first row compares elevation to eight other parameters. In AHP, parameters deemed more important receive higher numerical weights, while less important ones are assigned reciprocal values. For example, if basin elevation is more significant than slope, it may be assigned 5, with slope receiving 1/5. This reciprocal system ensures consistent and proportional weighting across all parameters for flood-susceptibility analysis (Saaty, 1977; Das, 2018).

The quantitative and qualitative approach is a major strength of AHP (Forman, 1993; Doke *et al*., 2021).

$$A = (aij)_{n*n} = \begin{bmatrix} a_{11} & a_{12} & ..a_{1n} \\ a_{21} & a_{22} & ..a_{21} \\ a_{n1} & a_{n2} & ..a_{nn} \end{bmatrix}, a_{ii=}1, a_{ij}$$

$$= \frac{1}{a_{ij}}, a_{ij} \neq 0 \qquad (2)$$

Where,

A: The matrix A represents the collection of all pairwise comparisons between the parameters n × n, indicating a square matrix with n rows and n columns.

$aij =$ Element at the i-th row and j-th column

a_{ii} =1: Diagonal elements of the matrix are always 1, as each parameter is equally important to itself

$a_{ij} = \frac{1}{a_{ij}}$: Elements are reciprocals of each other, ensuring consistency in the comparison (if parameter iii is more important than j, then j is less important than i).

$a_{ij} \neq 0$: No element in the matrix is zero, as comparisons are always non-zero values.

Afterward, the weighted arithmetic mean methodology is employed to compute the weights in the PCM. In this process, the values in the matrix are standardized to obtain the standardized values in the standard pairwise comparison matrix (Table 2). This normalization step confirms that all values are scaled in a consistent method, facilitating the calculation of relative importance or weights for each parameter. Using Equation (3), the pairwise comparison matrix (Table 1) was normalized by dividing each parameter by its respective column sum, ensuring all column totals equal to 1. The average of each row produced the relative weight of each criterion (Table 2). (Equation 3 and 4).

$$a_{ij} = \frac{a_{ij}}{\sum_{i=1}^{n} a_{ij}} \quad (3)$$

$$w_i = \frac{1}{n} \sum_{j=n}^{n} a'_{ij} \quad (4)$$

$$A_w = \lambda max\, W \quad (5)$$

The equation $A_w = \lambda max\, W$ is used to find the importance of criteria in decision-making. w is the weight factor and A is a comparison matrix, and. By averaging rows and solving the equation, we determine the relative weights of each criterion (Equation 5).

3.1.1 Consistency ratio (CR)

Consistency in judgments is assessed using the CR calculated as (Biswas *et al*., 2021),

$$\text{CR} = \frac{CI}{RI} \quad (6)$$

Where the Consistency Index,

$$\text{CI} = \frac{\lambda_{max} - n}{n-1} \quad (7)$$

λ *max* as the largest eigenvalue and n as the matrix order (Pawluszek and Borkowski, 2017).

Equation (7) was then applied to assess judgment consistency. The maximum eigenvalue (λ_{max}=13.78)) was derived from the matrix–weight product, yielding (CI=0.065) and (CR=0.041). As CR < 0.10, the pairwise comparisons are considered consistent and reliable for flood susceptibility analysis in the KRB. Eigenvalues, particularly λ_{max}, are derived from the sum of total and normalized weights, with Saaty's RI providing consistency benchmarks, such as 1.56 for 13 criteria. Table 3 represents the AHP method has been applied to a total of 13 parameters and all their subtypes considered for the research, and those parameters have been given a relative ranking according to their importance.

3.2 Preparations of Thematic Layers

To delineate the flood hazard zones in the KRB, high-resolution satellite imagery and ancillary data were procured from a range of digital repositories and governmental institutions. The detailed methodological framework is illustrated in Figure 2.

3.2.1 Elevation

According Botzen *et al* (2012) elevation is key factor in mapping flood risk vulnerability. High elevated land areas have less risk of flooding, while lowland plains are more vulnerable. The areas at higher elevations exhibits lower flood susceptibility (Tehrany *et al*., 2013; Das, 2018). The relief in Krishna basin ranges from 0 to 1865m. About 10% of the basin lies around 250m elevation, while nearly 20% of the area falls between 250 and 450m (Figure 3a).

3.2.2 Slope

Mapping flood-susceptible areas, slope is a crucial topographic factor because it controls surface water flow. In the present study area, the slope values range from 0° to 67°. Surface slope acts as an amplifying factor by increasing water-flow velocity and reducing infiltration, which collectively heightens flood risk (Elkhrachy, 2015). As the slope gradient increases, runoff becomes faster and infiltration decreases; however, where the slope suddenly flattens, the reduced flow velocity causes water to accumulate, leading to stagnation and potential flooding (Das, 2019; Doke *et al*., 2021).

3.2.3 Distance from the river

Proximity to river channels is considered a significant geomorphic factor while preparing accurate scientific maps of flood prone area. The areas closer to the river generally have lower elevation and gentler slopes. Additionally, a river channel represents the lowest topographic point within a given area. Consequently, regions located farther from the river exhibit reduced susceptibility to flooding. In the present study the buffer tool of ArcGIS software is used to calculate the distance from the river (Figure 3c). Multiple buffers were generated at intervals of 0.5km, which were then merged into a single vector layer and subsequently converted into a raster format for further analysis. (Fernandez and Lutz, 2010; Das, 2018). Flooding raises groundwater levels, especially in flat areas, causing prolonged waterlogging and slower drainage. However, the areas near rivers, ponds, and lakes are prone to flooding due to elevation changes, with flash floods also occurring based on meteorological and topographical factors (Pham *et al*., 2020).

Table 1. Pairwise comparison matrix (PCM)

Criteria	Elevation	Slope	Distance from Drainage	Geomorphology	DD	FA	RF	LULC	Geology	ST	STI	TWI	Curvature
Elevation	1												
Slope	1/2	1											
Distance from Drainage	1/3	1/2	1										
Geomorphology	1/4	1/3	1/2	1									
DD	1/4	1/4	1/3	1/2	1								
FA	1/5	1/4	1/4	1/3	1/2	1							
RF	1/6	1/5	1/4	1/4	1/3	1/2	1						
LULC	1/7	1/6	1/5	1/4	1/4	1/3	1/2	1					
Geology	1/8	1/7	1/6	1/5	1/4	1/4	1/3	1/2	1				
ST	1/8	1/8	1/7	1/6	1/5	1/4	1/4	1/3	1/2	1			
STI	1/9	1/8	1/8	1/7	1/6	1/5	1/4	1/4	1/3	1/2	1		
TWI	1/9	1/9	1/8	1/8	1/7	1/6	1/5	1/4	1/4	1/3	1/2	1	
Curvature	1/10	1/9	1/9	1/8	1/8	1/7	1/6	1/5	1/4	1/4	1/3	1/2	1

*DD-Drainage Density, FA-Flow Accumulation, RF-Rainfall, LULC-Land Use Land Cover, ST- Soil Texture, STI-Stream Power Index, TWI-Topographic Wetness Index.

Table 2. Standardized pairwise comparison matrix and their weights

Criteria	Elevation	Slope	Distance from Drainage	Geomorphology	DD	FA	RF	LULC	Geology	ST	STI	TWI	Curvature	Weights	Weights %
Elevation	0.3096	0.3831	0.3659	0.3309	0.2505	0.2399	0.2247	0.2088	0.1936	0.1630	0.1556	0.1353	0.1316	0.2379	23.79
Slope	0.1548	0.1916	0.2439	0.2481	0.2505	0.1919	0.1873	0.1789	0.1694	0.1630	0.1383	0.1353	0.1184	0.1824	18.24
Distance from Drainage	0.1032	0.0958	0.1220	0.1654	0.1879	0.1919	0.1498	0.1491	0.1452	0.1426	0.1383	0.1203	0.1184	0.1408	14.08
Geomorphology	0.0774	0.0639	0.0610	0.0827	0.1252	0.1440	0.1498	0.1193	0.1210	0.1222	0.1210	0.1203	0.1053	0.1087	10.87
DD	0.0774	0.0479	0.0407	0.0414	0.0626	0.0960	0.1124	0.1193	0.0968	0.1019	0.1038	0.1053	0.1053	0.0854	8.54
FA	0.0619	0.0479	0.0305	0.0276	0.0313	0.0480	0.0749	0.0895	0.0968	0.0815	0.0865	0.0902	0.0921	0.0660	6.60
RF	0.0516	0.0383	0.0305	0.0207	0.0209	0.0240	0.0375	0.0596	0.0726	0.0815	0.0692	0.0752	0.0789	0.0508	5.08
LULC	0.0442	0.0319	0.0244	0.0207	0.0157	0.0160	0.0187	0.0298	0.0484	0.0611	0.0692	0.0602	0.0658	0.0389	3.89
Geology	0.0387	0.0274	0.0203	0.0165	0.0157	0.0120	0.0125	0.0149	0.0242	0.0407	0.0519	0.0602	0.0526	0.0298	2.98
STI	0.0387	0.0239	0.0174	0.0138	0.0125	0.0120	0.0094	0.0099	0.0121	0.0204	0.0346	0.0451	0.0526	0.0233	2.33
STI	0.0344	0.0239	0.0152	0.0118	0.0104	0.0096	0.0094	0.0075	0.0081	0.0102	0.0173	0.0301	0.0395	0.0175	1.75
TWI	0.0038	0.0213	0.0152	0.0103	0.0089	0.0080	0.0075	0.0075	0.0060	0.0068	0.0086	0.0150	0.0263	0.0112	1.12
Curvature	0.0034	0.0024	0.0136	0.0103	0.0078	0.0069	0.0062	0.0060	0.0060	0.0051	0.0057	0.0075	0.0132	0.0072	0.72

Table 3. The pairwise comparison matrix and the weights according to sub-criteria

Sr. No	Parameter	Sub-Class	1	2	3	4	5	6	7	8	9	CR	Weights	Weights (%)
1	Elevation	0 – 268	1									0.0947	0.499	50
		268 – 467	1/3	1									0.256	26
		467 – 608	1/5	1/3	1								0.138	14
		608 – 786	1/7	1/5	1/3	1							0.070	7
		786 – 1865	1/8	1/6	1/5	1/3	1						0.038	4
2	Slope (Degree)	0 – 2.1	1									0.0788	0.393	40
		2.1 – 5.8	1/2	1									0.296	30
		5.8 – 12.2	1/3	1/3	1								0.166	17
		12.2 – 21.4	1/4	1/4	1/3	1							0.093	9
		21.4 – 67.4	1/5	1/5	1/4	1/3	1						0.051	5
3	Distance from Drainage (Km)	0 – 0.5	1									0.0609	0.445	45
		0.5 – 1	1/2	1									0.297	30
		1 – 2	1/4	1/3	1								0.147	
		2 – 3	1/6	1/5	1/3	1							0.073	7
		3 – 5	1/8	1/7	1/5	1/3	1						0.037	4
4	Geomorphology	Water body	1									0.0414	0.3070	31
		Flood Plain	1/2	1									0.2182	22
		Older Flood Plain	1/3	1/2	1								0.1543	15
		Deltaic Plain	1/4	1/3	1/2	1							0.1089	11
		Alluvial Plain	1/4	1/4	1/3	1/2	1						0.0764	8
		Middle Level Plateau	1/5	1/4	1/4	1/3	1/2	1					0.0533	5
		High Level Plateau	1/5	1/5	1/4	1/4	1/3	1/2	1				0.0370	4
		Highly Dissected Hills and Valleys	1/6	1/5	1/5	1/4	1/4	1/3	1/2	1			0.0259	3
5	Drainage Density	Very High	1									0.0341	0.464	46
		High	1/2	1									0.264	26
		Moderate	1/4	1/2	1								0.149	15
		Low	1/6	1/4	1/2	1							0.083	8
		Very Low	1/8	1/6	1/5	1/2	1						0.040	4
6	Flow Accumulation	77311428 – 228338405	1									0.0642	0.441	4

		37756744 – 77311428	1/2	1								0.249	25
		77080431 – 37756744	1/4	1/2	1							0.179	18
		4494850 – 17080431	1/5	1/3	1/3	1						0.090	9
		0 – 4494850	1/6	1/5	1/5	1/3	1					0.046	4
7	Rainfall (mm)	< 980	1								0.0207	0.456	46
		981 - 1315	1/2	1								0.254	25
		1315 - 1912	1/4	1/2	1							0.157	16
		1912 - 2773	1/5	1/3	1/2	1						0.087	9
		>2773	1/7	1/5	1/4	1/2	1					0.049	5
8	LULC	Water body	1								0.0357	0.376	38
		Built-up	1/2	1								0.246	25
		Westland	1/3	1/2	1							0.145	15
		Agriculture Land	1/4	1/3	1/2	1						0.108	11
		Grass Land	1/5	1/4	1/3	1/2	1					0.064	6
		Forest Land	1/6	1/5	1/5	1/4	1/2	1				0.043	4
9	Geology	Deccan Trap	1								0.0413	0.273	27
		Dharwar	1/2	1								0.182	18
		Cuddapah	1/2	1/2	1							0.189	19
		Gondwana	1/3	1/3	1/2	1						0.123	12
		Granite	1/4	1/5	1/3	1/2	1					0.085	9
		Kaladgi	1/5	1/5	1/5	1/3	1/2	1				0.061	6
		Pakhal	1/7	1/6	1/6	1/4	1/3	1/2	1			0.042	4
		Eastern Ghat	1/7	1/7	1/7	1/6	1/5	1/4	1/3	1		0.027	3
		Peninsular Gneissic Complex	1/8	1/7	1/7	1/7	1/6	1/6	1/4	1/3	1	0.018	2
10	Soil Texture	Clay	1								0.0413	0.273	27
		Clay Loam	1/2	1								0.182	18
		Loam	1/2	1/2	1							0.189	19
		Silty Clay	1/3	1/3	1/2	1						0.123	12
		Silty Clay Loam	1/4	1/5	1/3	1/2	1					0.085	9
		Silty Loam	1/5	1/5	1/5	1/3	1/2	1				0.061	6
		Loamy Sand	1/7	1/6	1/6	1/4	1/3	1/2	1			0.042	4

		Fine Sand Loamy	1/7	1/7	1/7	1/6	1/5	1/4	1/3	1			0.027	3
		Sandy Loam	1/8	1/7	1/7	1/7	1/6	1/6	1/4	1/3	1		0.018	2
11	SPI	8.9 – 9.5	1									0.0947	0.499	50
		9.5 – 10.8	1/3	1									0.256	26
		10.8 – 12.9	1/5	1/3	1								0.138	14
		12.9 – 16.2	1/7	1/5	1/3	1							0.070	7
		16.2 – 23.7	1/8	1/6	1/5	1/3	1						0.038	4
12	TWI	11.3 – 23.8	1									0.0357	0.459	46
		8.01 – 11.3	1/2	1									0.268	27
		5.6 – 8.01	1/4	1/2	1								0.144	14
		3.7 – 5.6	1/6	1/4	1/2	1							0.085	9
		-0.7 – 3.7	1/7	1/6	1/4	1/3	1						0.043	4
13	Curvature	-3.8 – -2.1	1									0.0835	0.503	50
		-2.1 – -0.05	1/3	1									0.260	26
		-0.05 – 0.05	1/5	1/3	1								0.134	13
		0.05 – 0.25	1/7	1/5	1/3	1							0.068	7
		0.25 – 3.7	1/9	1/7	1/5	1/3	1						0.035	4

3.2.4 Geomorphology

Geomorphology affects both groundwater and flooding by influencing how water moves, collects, and drains in an area. Geomorphology regulates groundwater dynamics by controlling infiltration, storage, and movement, with floodplains enhancing recharge but increasing flood risk, while hilly terrains promote runoff and flash floods (Andualem and Demeke, 2019; Doke *et al*., 2021). The Figure 3d shows nine geomorphic features of the KRB, including waterbodies, flood plain, older flood plains, deltaic plains, alluvial plains, high-level plateaus, middle-level plateaus, and dissected hills and valleys (Bordoloi *et al*., 2023). High flood susceptibility in its flood plain, older flood plain, deltaic plain, and alluvial plain due to low elevation, flat topography, and proximity to river systems. The deltaic plain is particularly vulnerable due to tidal influences and sediment deposition. In contrast, high-level plateaus, middle-level plateaus, and dissected hills and valleys facilitate rapid runoff, intensifying downstream flooding.

3.2.5 Drainage density

Drainage density (Dd), defined as the ratio of total drainage network length to total basin area, influences flood risk. Higher drainage density results in faster runoff, lower infiltration and increased flood potential, especial in steep or impermeable areas. Low drainage density allows greater infiltration, reducing flood susceptibility. However, while high Dd increases flood risk, it also aids in rapid water evacuation, with overall impact depending on soil permeability, land use, and rainfall intensity. (Subbarayan and Sivaranjani, 2020; Doke *et al*., 2021). Hence, higher Dd areas are assigned higher scores due to their greater flood susceptibility, while areas with lower drainage density received lower scores as they have reduced flood risk. The Dd in the study area ranges between 0 to 1.49 km/km². They are divided into five categories to capture finer spatial variations in drainage density and to improve the clarity and accuracy of the flood-susceptibility analysis (Figure 3e).

3.2.6 Flow accumulation

Flow accumulation is defined as concentration of flow within a watershed, representing the sum of upstream area contributing runoff to a specific point. In the downstream region of river, where tributaries converge, the velocity and volume of water increase, which rises the flood potential. Flow accumulation measures drainage areas and increases from high land to river outlets (Schauble *et al*., 2008). The upstream region of river Krishna the flow accumulation is lesser due to the presence of lower-order streams (Figure 3f). As the river progresses downstream, numerous tributaries merge with the main channel, significantly increasing flow accumulation and flood vulnerability (Krishnan *et al*., 2025). Therefore, higher flow accumulation in the downstream region increases flood risk (Tehrany *et al*., 2015; Das, 2018).

3.2.7 Rainfall

River water level and flow accumulation depends on the intensity, frequency, and amount of rainfall (Dou *et al*., 2017). Precipitation is the major source of surface water, excluding glacier-fed areas. It plays a crucial role in river flow and flooding, with sudden rainfall, especially in dry regions, potentially triggering flash floods (Das, 2018). However, groundwater is a vibrant natural reserve refilled by precipitation. While intense rainfall enhances surface water penetration, excessive rainwater can decrease the soil's absorption ability, leading to increased runoff and a greater possibility of flooding (Maity and Mandal, 2019; Doke *et al*., 2021). The basin receives ~90% of its 859 mm annual rainfall during the southwest monsoon (June–October) (Figure 4g). Orographic lifting of monsoon winds by the Western Ghats (610–2,134 m) causes high rainfall in the western basin, while the eastern regions remain drier (WRIS, 2018). This spatial variability, combined with intense monsoon precipitation, exacerbates flood risks, particularly in downstream areas with inadequate drainage and high sediment loads.

3.2.8 Land use land cover (LULC)

LULC is important for flood risk mapping because it affects surface runoff, infiltration, and the connection between surface water and aquifer (Gigovic *et al*., 2017; Kazakis *et al*., 2015). LULC data has been collected from the Bhuvan Portal, a website of the National Remote Sensing Centre ISRO, Hyderabad, India. This dataset is for the period 2019–2020 and has been published under the National Land Use and Land Cover Mapping Project. The maps are based on Level-II classification system and have a scale of 1:50,000. Land utilization patterns in the Krishna Basin are shaped by socio-cultural and economic factors, influencing adaptive land use techniques in response to the natural environment (Das *et al*., 2017; Kaur *et al*., 2017). Urban landscape planning plays a vital role in environmental sustainability by supporting better management of land changes over time while mitigating the risks of natural calamities i.e. floods, caused by deforestation and urbanization. (Cetin *et al*., 2018a; Cetin *et al*., 2018b; Das *et al*., 2017). The basin exhibits diverse land use classes, including agriculture (75.86%), natural vegetation (10.04%), wetlands (7.64%), water bodies (4.07%), built-up areas (2.29%), and grasslands (0.11%) (Figure 4h).

3.2.9 Geology

Porosity and permeability, governed by rock lithology, plays a critical role in controlling infiltration, runoff generation, and groundwater flow (Kalita *et al*., 2025).

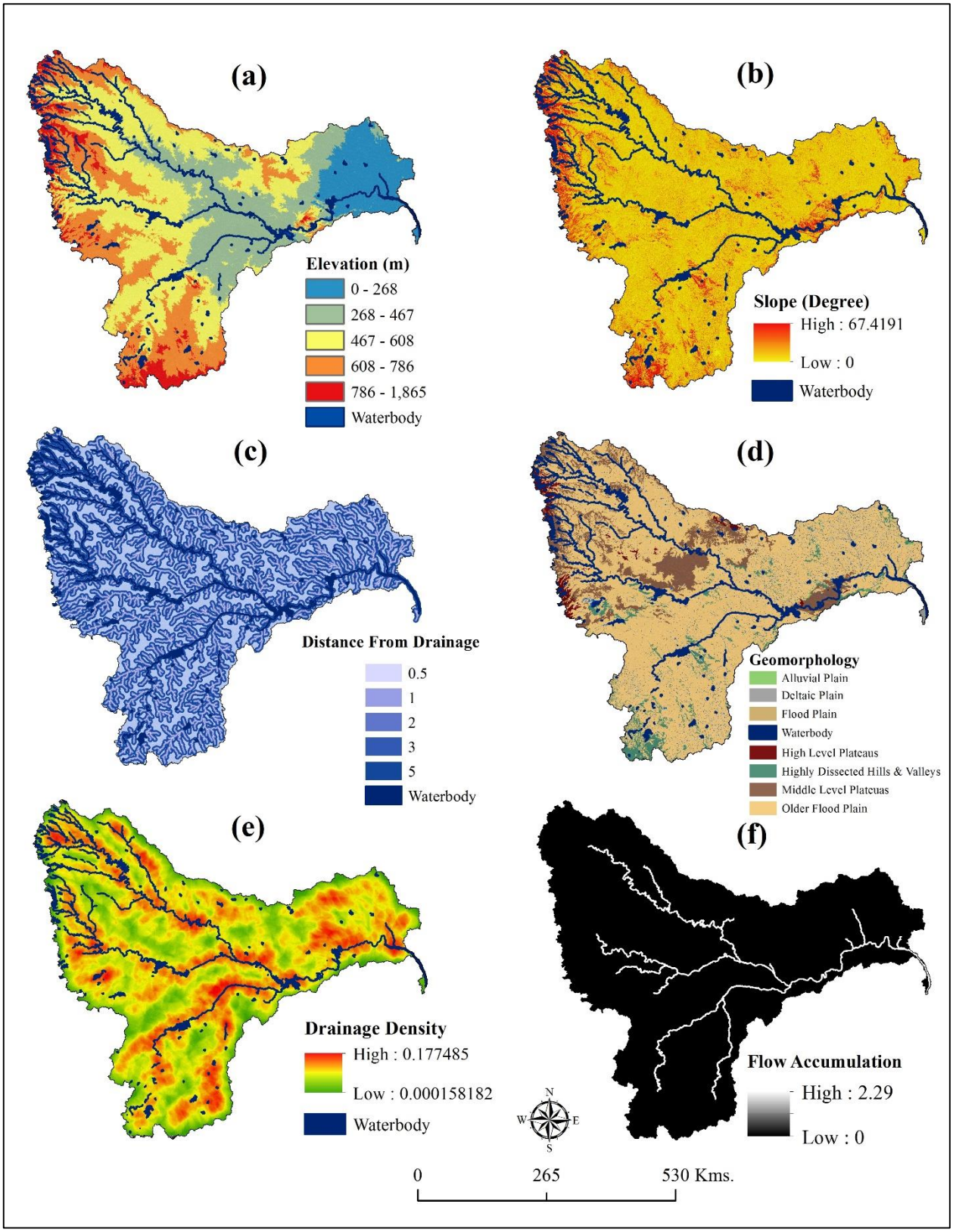

Figure 3. A responsible factors: a) Elevation, b) Slope, c) Distance from the stream, d) Geomorphology, e) Drainage Density, f) Flow Accumulation.

Lithology can significantly impact flood behavior particularly in basaltic terrains such as the Deccan Traps where low porosity and limited permeability promote quick surface runoff, reduced infiltration, and unstable channel conditions (Kale and Rajaguru, 1987; Subramanian, 1993; Grover *et al*., 2024; Terker, 2024). Although precipitation, surface morphology, and land use often exert stronger controls on short-term flood intensity, lithological characteristics still contribute significantly to basin-scale hydrological response. In

fact, several recent studies have shown that Deccan basalt formations enhance runoff generation and increase flood susceptibility due to their unique hydraulic properties (Jerin Joe, *et al*., 2025; Paswan *et al*., 2025). Geological information for this study was obtained from the GSI, based on digital geological maps at 1:250,000 scale, which provide a reliable overview of lithological variability across the study area. The basin comprises three major geological units the Deccan Trap basalt, Cuddapah sediments, and Dharwad crystalline rocks (Figure 4i). The northwestern Deccan Trap region, dominated by hard basaltic flows, shows low permeability and high runoff, particularly in the upper catchments of the Mula, Mutha, Bhima, Pavana, and Indrayani rivers. In contrast, the Cuddapah region exhibits moderate to high infiltration, supporting groundwater recharge, while the Dharwad crystalline terrain allows deeper percolation due to its fractured bedrock. Additional lithologies such as Gondwana, Granite, Kaladgi, and Pakhal further contribute to the basin's geological and hydrological diversity.

3.2.10 Soil type

Soil type is a key factor in influencing surface runoff and the infiltration rate of water. Soils with higher clay content than sand, the amount and rate of surface runoff are generally greater (Olii *et al*., 2021). Soil data has been obtained from the online resource of National Bureau of Soil Survey and Land Use Planning (NBSS and LUP). This dataset is at a scale of 1:250,000 and shows the major soil types and soil properties of the study area. The KRB exhibits various soil classes, such as clay loam, fine sandy loam, loamy sand, loam, and clay, each distributed across different regions of the basin (Figure 4j). Clay loam and clay soils are found in large quantities in the north-western part of the KRB. The presence of the Deccan trap in this region is the rate of erosion intensity and of water velocity is high with water infiltration rate is low (Jain *et al*., 2007; Patil *et al*., 2024). Fine sandy loam in the central and eastern parts of the KRB represents mature to old alluvial deposits, where long-term sediment sorting produces smooth, fine-textured soils. These well-developed alluvial surfaces reduce channel roughness and lower river velocity, but their broad, gently sloping floodplains allow the river to carry a higher volume of water (Leopold and Wolman, 1970; Bridge, 2009). The loamy sand soil is situated in the south-western area of the basin, influenced by the Western Ghats, and is shaped by moderate river flow from the tributaries.

3.2.11 Stream power index

The SPI measures the erosive power of water flow (Jebur *et al*., 2014; Khosravi *et al*., 2016; Das, 2019; Yilmaz, 2022), assessing the energy available for sediment transport and erosion in rivers. This energy influences channel changes and plays significant role in flood events (Das and Scaringi, 2021). SPI is an important measure of erosion and sediment transport in streams (Fuller, 2008; Barker *et al*., 2009; Hong *et al*., 2018). The SPI is calculated using the formula (Moore *et al*., 1991; Dejen and Soni 2021), as follows:

$$SPI = As\ tan\beta \quad (7)$$

Where, *As* is the specific catchment area, and β is the slope gradient.

The SPI of the KRB ranges from 8 to 23.8, indicating variations in flow energy and erosion potential across the watershed (Figure 4k). Higher SPI values suggest areas with intense water flow and increased erosion risk, often corresponding to steep slopes and major drainage channels, while lower values indicate regions with gentle slopes and decreases the flow intensity.

3.2.12 Topographic wetness index

TWI deals with how terrain affects surface water flow accumulation, soil saturation, and soil moisture, with high values in valleys and low values on slopes (Gokceoglu *et al*., 2005; Yong *et al*., 2012; Mojaddadi *et al*., 2017). Flooding is more likely in high TWI areas due to increased soil saturation, rising groundwater, and reduced drainage (Ho-Hagemann *et al*., 2015). TWI helps identify flood-prone areas by indicating zones with a higher potential for soil saturation, especially where low slopes and large contributing catchments promote water accumulation during heavy rainfall. The TWI is calculated as:

$$TWI = \ln(\mathrm{As}/\tan\beta) \quad (8)$$

Where, *As* = upslope contributing area ($m^2\ m^{-1}$), and β = the local slope inclination in degree.

Higher TWI values indicate areas with more water accumulation, which are more prone to flooding and higher soil moisture. Lower TWI indicates drier, well-drained areas with less risk of flooding. TWI values in the KRB range from –0.70 to 23.85. Although TWI is usually positive; negative TWI values represent ridge tops and steep slopes where water quickly runs off and little to no saturation occurs (Figure 4l).

3.2.13 Curvature

Curvature is commonly classified into concave, convex, and flat surfaces (Tehrany *et al*., 2013). Concave areas facilitate convergent flow, convex areas cause divergent flow, while flat surfaces produce minimal runoff (Costache and Tien, 2019). Curvature therefore helps interpret how terrain shape influences water movement across the landscape (Costache *et al*., 2020). These characteristics are crucial for hydrological modeling. Curvature also influences flooding: negative values (concave) trap water, positive values (convex) promote drainage, and values near zero indicate flat areas with even water flow (Das, 2018; Cao *et al*., 2016). In the KRB, the general surface curvature ranges from –3 to 3.7, reflecting variations in overall landform shape that influence water flow, accumulation, and erosion across the basin (Figure 4m). Negative values represent concave areas, which promote water accumulation and increase

flood susceptibility, while positive values indicate convex regions, facilitating runoff and reducing flood risk.

All data sets have been unified to a spatial resolution of 90m by transforming them into the same coordinate system, WGS 84 / UTM Zone 43N, thereby maintaining spatial consistency across all datasets.

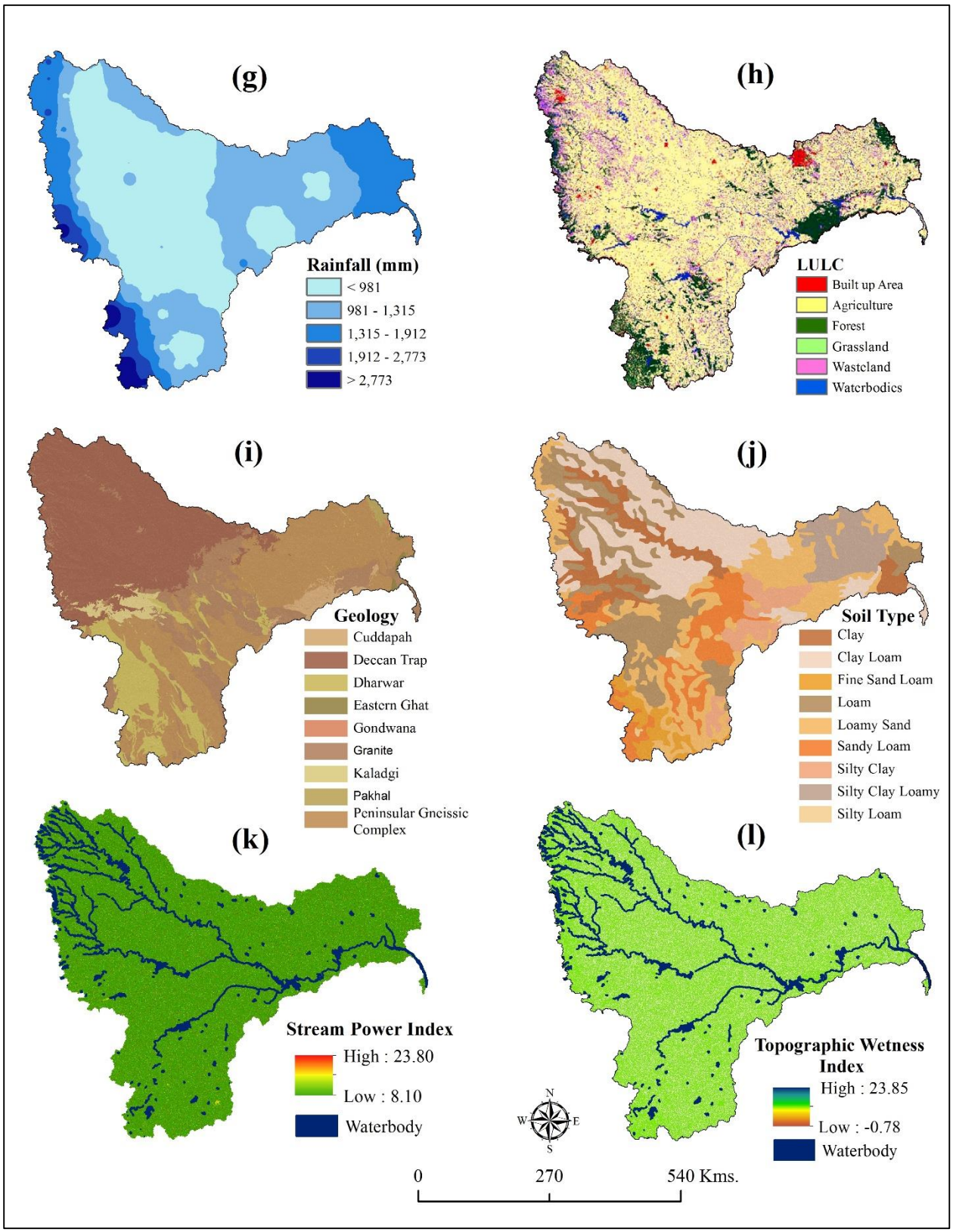

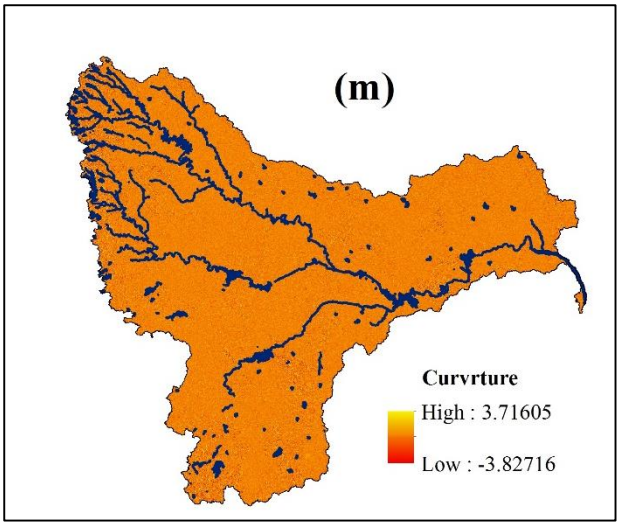

Figure 4. Responsible factors: g) Rainfall, h) Landuse and Land Cover, i) Geology, j) Soil Type, k) Stream Power Index (SPI), l) Topographic Wetness Index (TWI) and m) Curvature

3.3 Flood Susceptibility Mapping

Geomorphic parameters generated in ArcGIS 10.8 were used for flood-susceptibility analysis and for planning measures to manage peak flows during extreme rainfall. The significance of each parameter was evaluated using a pairwise comparison matrix within the AHP-based MCDM framework. The resulting weights were then integrated in a weighted overlay analysis in GIS to generate the flood-susceptibility map. This analytical approach provides a systematic and objective method for assessing flood risk and supporting ground-level planning for mitigation of natural and human-induced hazards. The resultant map was prepared and average scores were calculated and it was categorized into five classes. These classes were re-classified into five flood susceptible zone, i.e. as very low, low, moderate, high and very high (Figure 5) (Arabameri *et al*., 2020; Doke *et al*., 2021). Flood vulnerability is strongly controlled by local topography, surface runoff characteristics, and sediment transport processes. Areas classified as very high and high flood-susceptible zones are typically located in low-relief, flat floodplain regions. These areas tend to experience slower surface runoff, higher water accumulation, and increased rates of sediment deposition, which collectively intensify flood impacts (Mahmoud and Gan, 2018). Moderate susceptibility zones occur in areas of intermediate relief, where higher runoff and lower infiltration result in occasional, moderate flooding impacts. Low and very low susceptibility zones characterize steeply sloped regions with rapid runoff, reducing flood risks but limiting groundwater recharge and increasing soil erosion. About 19% of the total area of KRB is highly prone to flooding, most of which falls in the meander belts and floodplain zones of the river. These areas are characterized by gentle to moderate slopes, older floodplains, and a dense drainage network. Factors such as high flow accumulation, heavy rainfall, high runoff, and clay-loam soil further increase flood risk by limiting water absorption.

Additionally, 19% of the area falls within the high flood susceptibility zone, primarily located in the meander belts and floodplains. These regions are characterized by clay–loam soils, which have moderate permeability: they promote groundwater recharge under normal conditions but, during intense rainfall, their limited infiltration rate leads to rapid surface saturation. Combined with gentle slopes, moderate drainage density, and extensive agricultural land use, these factors reduce runoff dispersion and enhance water accumulation, thereby increasing overall flood susceptibility.

The moderate flood susceptibility zone (20%) is characterized by low flow accumulation, moderate drainage density, and greater distance from the main river channel. Areas located farther from the channel typically experience attenuated floodwaters because the depth and velocity of overbank flows decrease with increasing distance from the source (Knighton, 2014). As floodwater disperse across the floodplain, water spreads more thinly, infiltration increases, and the hydraulic impact is reduced (Ward and Robinson, 1975). Consequently, these areas exhibit moderate rather than high flood susceptibility. Factors such as average rainfall, extensive agricultural land, and high percolation capacity due to clay-loam soil contribute to its hydrological response, reducing flood intensity and promoting groundwater recharge.

The low (21%) and very low (21%) flood susceptible zones are mainly found in steep mountainous regions, far from major river channels (Figure 5). These areas exhibit low drainage density, resulting in fewer surface water pathways, which significantly reduces the likelihood of flooding. Despite experiencing high rainfall, the steep topography and dense forest cover caused rapid runoff dispersion and

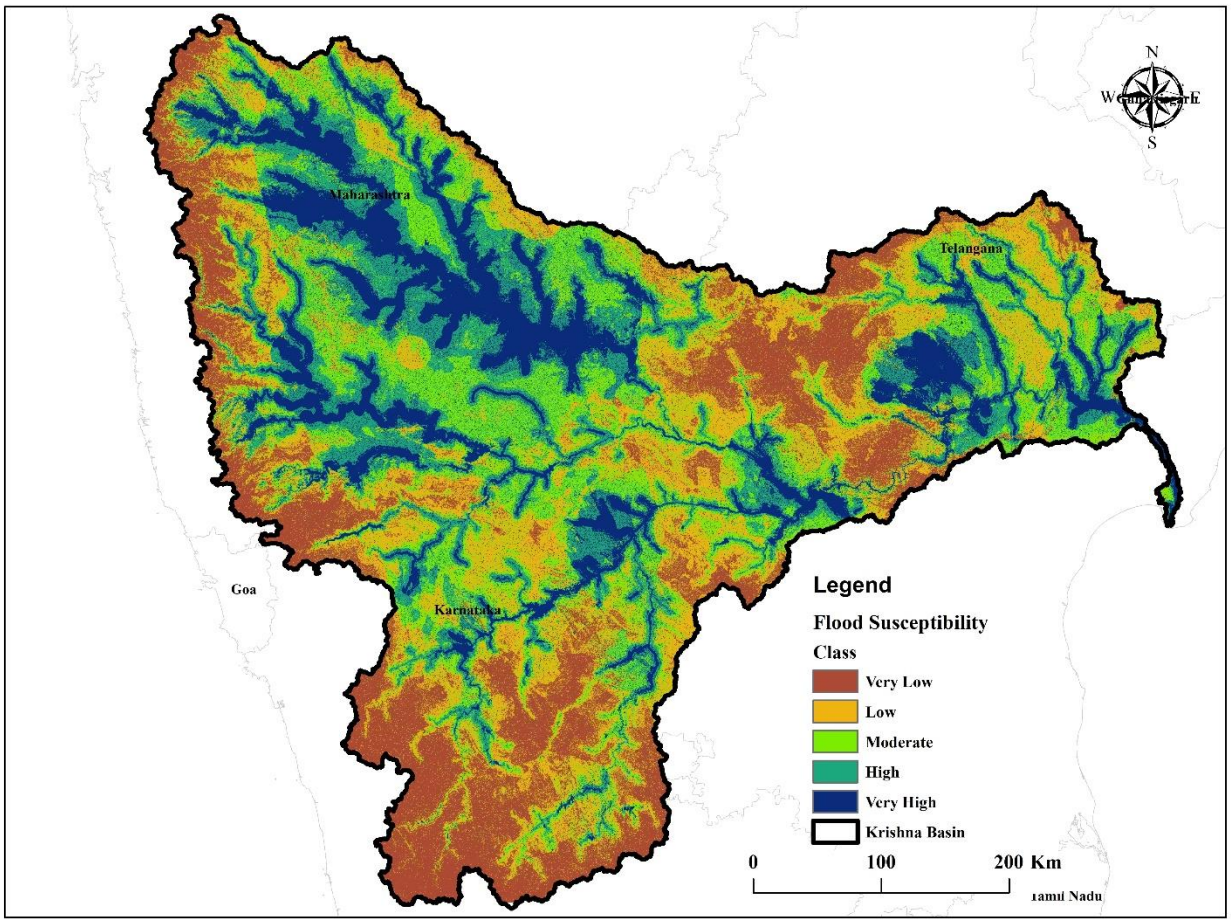

Figure 5. Flood susceptibility map of the study area.

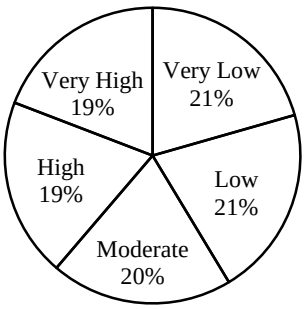

Figure 6. The pie chart shows the percentage of area under different flood-susceptibility categories.

enhance infiltration, effectively minimizing flood risk. Furthermore, the prevalence of natural vegetation helps stabilize slopes and regulate surface water flow, further contributing to reduced flood susceptibility in these zones.

The flood susceptibility maps are presented in a clear and accessible form, allowing users to interpret the results effectively even without specialized technical expertise. However, creating accurate flood maps requires a solid understanding of hydrology, geology, geomorphology, rainfall intensity, flow accumulation, slope, and remote sensing. It has been suggested that focusing on flood-prone and moderately prone areas can help reduce risks to communities, infrastructure, and agriculture (Bagyaraj *et al*., 2013; Diaz-Alcaide and Martinez-Santos, 2019; Murmu *et al*., 2019; Andualem and Demeke, 2019; Doke *et al*., 2021).

AHP is widely used for creating flood susceptibility maps worldwide. This technique helps in detecting areas that are high risk of flooding by analyzing various factors that contribute to flood risk (Kazakis *et al*., 2015; Hong *et al*., 2018; Subbarayan and Sivaranjani, 2020; Das and Scaringi, 2021). In addition, highly accurate demarcation of flood prone areas can be achieved using machine learning and real time flood forecasting (Khosravi *et al*., 2019; Islam *et al*., 2021; Tran *et al*., 2025; Wale *et al*., 2025). The analysis identifies Pune, Shirur, Daund, Phaltan, Baramati, Pandharpur, Solapur, Kolhapur, Sangli, Gokak, Mudhol, Jamkhandi, Bagalkot, Ilkal, Hubballi, Hosapete, Gangavati, Sindhnur, Devarakonda, Gadwal, Itikyal, Nalgonda, Anumula, Guntur, Nandigama, Madhira, Amaravati, Repalle, and Vijayawada are highly flood-prone cities (Table 4 and Figure 7).

However, intense rainfall over the Western Ghat regularly causes rapid inflows into major reservoirs such

as Koyna Dam, which has a live storage of approximately 2980 mm³ (Dhumal *et al.*, 2022). During high inflow events, controlled gate releases have surged to over 50,000 cusecs, significantly increasing the flow into the Krishna River (TOI, 2024). When these releases coincide with high river stages and narrow cross-sections downstream, they overwhelm the KRB, as supported by flood-inventory records documenting repeated flood events linked to large dam outflows. This confluence of urban infrastructure limitations, concentrated dam discharges, and seasonal rainfall leads to recurrent flooding, threatening communities and ecosystems in the region. These findings highlight the need for strengthened flood-management strategies, including improved urban drainage design, enhanced reservoir-operation protocols, and sustainable land-use planning. Specific measures such as establishing flood-retention reservoirs, implementing real-time discharge modelling, and expanding early-warning systems can significantly reduce downstream flood impacts. Future research should further examine flood susceptibility for applications in urban planning, disaster preparedness, and rainfall–runoff interactions to support evidence-based flood-risk management.

Table 4. The flood susceptible areas in KRB

Sr. No.	Basin name	High to very high flood susceptible areas
1	Bhima upper sub-basin	Pune, Shirur, Dound, Phaltan, Baramati, Pandharpur, and Solapur
2	Krishana upper sub-basin	Kolhapur, Sangli, Gokaka, Mudhol, Jamkhandhi, Bagalkot, Iikal
3	Tungbhadra upper basin	Hubballi, Hosapate
4	Tungbhadra lower basin	Gangavati, Sindhnur
5	Krishana middle sub-basin	Devarakonda, Gadwal, Itikyal, Nalgonda, Anumula, Guntur, Nandigama, Madhira, Amravati, Repelle, Vijaywada etc.

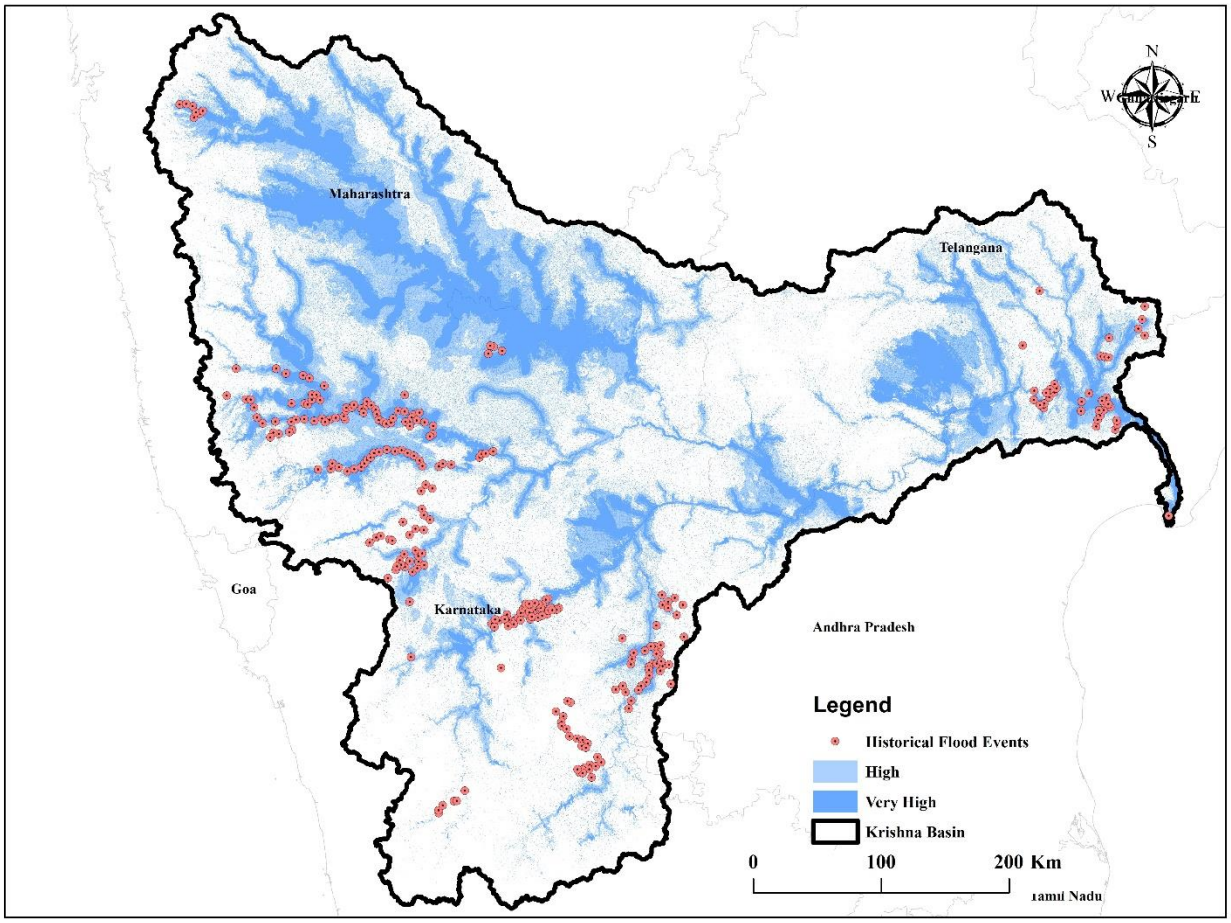

Figure 7. High and Very High flood susceptible areas with the red spot depicting the historical flood events in the Krishna basin.

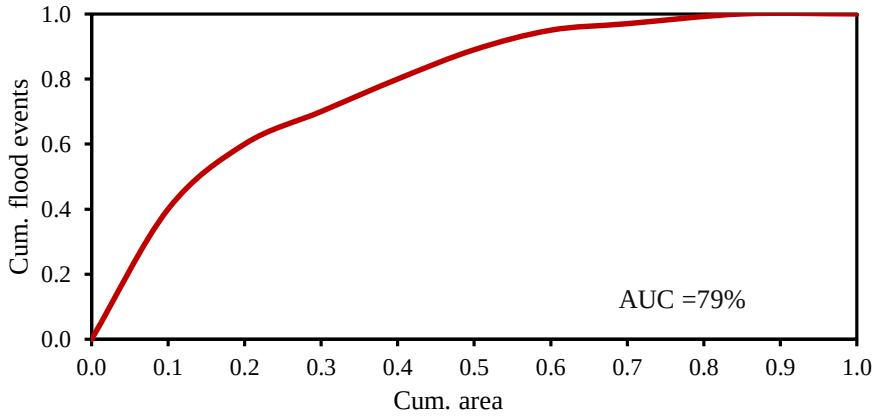

Figure 8. Area Under the Curve (AUC) shows considerably good accuracy (79%) of the predicted flood model.

3.4 Resultant map Validation

Worldwide numerous researchers have adopted different scientific methods for the result validation of geospatial analysis. Among them, the field survey method is considered as the most accurate and useful for direct validation. However, it is costly and time-consuming, so it is not feasible in every research (Das, 2019b).

Considering these limitations, validating the Flood Susceptibility map based on historical flood records (Historical Flood Inventory Data) is considered more convenient, effective and scientifically validated (Merz *et al*., 2007; Wang *et al*., 2022; Nguyen *et al*., 2024). The present research has used historical flood spatial data obtained from the Bhuvan Portal from 2009 to 2024 (a website of National Remote Sensing Centre, Government of India). Also, the report published in 2020 by the Water Resources Department of the Government of Maharashtra after a detailed review of the flood situation in the KRB in 2019 has been used as an important reference source for validation. For more scientific confirmation, information about flood-affected areas published in various newspapers has been used. Several mathematical and statistical approaches are commonly employed to validate such studies, including the Success Rate Curve (SRC), Area Under the Curve (AUC), Chi-square test, and flood density analysis (Kayastha *et al*., 2013).

In the present study, flood susceptibility analysis was carried out based on the AHP Model. Point data of 283 different flood-affected locations in the entire KRB has been prepared by the researcher, and this data has been considered as flood inventory data. Based on this data, a scientific method was adopted for validation of the flood susceptibility. The flood susceptibility map was classified into 20 classes. Then, the flood inventory data was overlayed on this map and computed an AUC, through which the accuracy of the map was evaluated.

The bivariate and multivariate statistical methods, frequency ratio models, and machine learning methods are considered scientifically effective for flood analysis; although the machine learning method is complex, it is widely used for high accuracy prediction of locations (Tehrany *et al*., 2015 a, b; Chen *et al*., 2017a, b). Compared to the machine learning method, the method adopted in the present research is more relevant and accurate to confirm the flood analysis point of view.

In comparison, the AHP method adopted in the present research is relatively simple, effective and scientifically validated for flood sensitivity analysis. Since the CR value obtained by this method is 0.04 and the AUC value is 79%, it is clear that the results of this research are highly reliable, statistically proven and useful for geographical analysis of flood risk.

4 CONCLUSION

In recent time, GIS and RS technologies are reducing costs and saving time. The flood susceptibility of a region depends directly or indirectly on various environmental factors. In the present study total 13 parameters i.e. Elevation, slope, distance from drainage, geomorphology, drainage density, flow accumulation, rainfall, land use and land cover, geology, soil type, SPI, TWI, and curvature where integrated into ArcGIS platform to delineate the potential flood-affected areas were determined. The scientific analysis of the flood susceptibility of KRB has been done based on the methods of geospatial techniques and AHP. This analysis is useful for flood management and disaster management preparedness as well as for immediate decision-making. Moreover, this method helps in making decisions regarding land use, infrastructure and flood prevention. It is also used to predict future flood conditions, financial planning and heavy rainfall.

The study revealed that, within the Krishna River Basin, 19% of the area falls under very high flood susceptibility, another 19% under high susceptibility, 20% under moderate susceptibility, and the remaining 42% under low to very low flood susceptibility. This research has shown that around 30 major settlements in the KRB fall in the very high and high flood susceptibility areas i.e. Kolhapur, Athni, Pandharpur, Solapur, Afzalpur, Pune, Hubballi, Hospete, Sindhnur, Gadwal, Nalgonda, Devarakonda, Khammam, Vijaywada, Guntur, etc. This means that these areas are at high risk of flooding and can have a major impact on

infrastructure, agriculture and settlements. Therefore, flood mitigation measures and proper planning are necessary for these areas. This study is scientifically conducted and can therefore be useful in guiding future flood management. To the scientific study in future flood conditions real-time data and machine learning technologies can be useful for accurately analyzing and mapping flood prone area as well as for modelling and monitoring flood conditions. This study has certain limitations. The use of generalized secondary data may reduce local accuracy, and the AHP method involves subjective expert judgment that can influence results. Moreover, while RS and GIS provide broad-scale assessments, higher accuracy would require detailed field validation, which is resource-intensive. Thus, the methods adopted in the present study have the capacity to assist as a useful guideline for flood management. Additionally, this approach can be implemented in similar studies across different regions globally.

The results can guide planners and disaster managers in identifying high-risk flood zones, improving early warning systems, and implementing land-use controls in vulnerable areas to reduce flood impact.

DECLARATION OF INTERESTS

The authors declare that they have no known competing financial interests or personal relationships that could have appeared to influence the work reported in this paper. The authors declare the following financial interests/personal relationships which may be considered as potential competing interests.

ACKNOWLEDGEMENT

We sincerely thank the faculty of the Department of Geography, S. N. Arts, D. J. Malpani Commerce, and B. N. Sarda Science College (Autonomous), Sangamner, Ahilyanagar, for their guidance and support. The facilities and encouragement provided by the institute were invaluable in completing this work. Further, the authors are thankful to the anonymous reviewers and the handling editor for reviewing this manuscript and for their constructive comments, which significantly improved the quality of the work.

ABBREVIATIONS

AHP: Analytical Hierarchy Process; **AUC**: Area Under Curve; **CI**: Consistency Index; **CR**: Consistency Ratio; **DD**: Drainage Density; **DEM**: Digital Elevation Model; **FA**: Flow Accumulation; **GIS**: Geographical Information System; **GSI**: Geological Survey of India; **IMD**: Indian Meteorological Department; **KRB**: Krishna River Basin; **LULC**: Land Use and Land Cover; **NBSS** and **LUP**: National Bureau of Soil Survey and Land Use Planning; **PCM**: Pairwise Comparison Matrix; **RF**: Rainfall; **RS**: Remote Sensing; **SPI**: Stream Power Index; **SRC**: Success Rate Curve; **SRTM**: Shuttle Radar Topography Mission; **ST**: Soil Texture; **TWI**: Topographic Wetness Index.

CONFLICT OF INTEREST STATEMENT

We, the undersigned authors, hereby declare that the research paper titled “Assessment of Flood Susceptibility Mapping in the Krishna River Basin Using Geospatial Techniques.” is an original work conducted by us. We confirm that this paper has not been previously submitted or published in any other journal or platform, nor is it currently under review elsewhere all sources, data, and references used in this research have been appropriately acknowledged. Furthermore, we confirm that all authors have contributed significantly to the work and have agreed to the final version of the manuscript for submission. No potential conflict of interest was reported by the authors.

FUNDING SOURCE

This study received no external funding.

REFERENCE

Abijith, D., Saravanan, S., Parthasarathy, K. S. S., Reddy, N. M., Niraimathi, J., Bindajam, A. A. and Abdo, H. G., 2025. Assessing the impact of climate and land use change on flood vulnerability: A machine learning approach in coastal region of Tamil Nadu, India. *Geoscience Letters*, 12(1), 1. DOI: https://doi.org/10.1186/s40562-025-00377-7

Al-Ruzouq, R., Shanableh, A., Jena, R., Gibril, M. B. A., Hammouri, N. A. and Lamghari, F., 2024. Flood susceptibility mapping using a novel integration of multi-temporal sentinel-1 data and eXtreme deep learning model. *Geoscience Frontiers*, 15(3), 101780. DOI: https://doi.org/10.1016/j.gsf.2024.101780

Andualem, T. G. and Demeke, G. G., 2019. Groundwater potential assessment using GIS and remote sensing: A case study of Gunatana landscape, upper blue Nile Basin. *Journal of Hydrology: Regional Studies*, 24, 100610. DOI: https://doi.org/10.1016/j.ejrh.2019.100610

Arabameri, A., Saha, S., Chen, W., Roy, J., Pradhan, B. and Bui, D. T., 2020. Flash flood susceptibility modelling using functional tree and hybrid ensemble techniques. *Journal of Hydrology*, 587, 125007. DOI: https://doi.org/10.1016/j.jhydrol.2020.125007

Arora, A., 2023. Flood susceptibility prediction using multi criteria decision analysis and bivariate statistical models: A case study of Lower Kosi River Basin, Ganga River Basin, India. *Stochastic Environmental Research and Risk Assessment*, 37, 1855–1875. DOI: https://doi.org/10.1007/s00477-022-02370-4

Arora, A., Durga G, P., Pandey, M. and Arabameri, A., 2025. Machine learning model optimization for flood susceptibility zonation over the Kosi megafan, Himalayan foreland basin, India. *Scientific Reports*, 15(1), 32757. DOI: https://doi.org/10.1038/s41598-025-07403-w

Atif, S., Umar, M. and Ullah, F., 2021. Investigating the flood damages in Lower Indus Basin since 2000: Spatiotemporal analyses of the major flood events. *Natural Hazards*, 108, 2357–2383. DOI: https://doi.org/10.1007/s11069-021-04783-w

Bagyaraj, M., Ramkumar, T., Venkatramanan, S. and Gurugnanam, B., 2013. Application of remote sensing and GIS analysis for identifying groundwater potential zone in parts of Kodaikanal Taluk, South India. *Frontiers of Earth Science*, 7, 65–75. DOI: https://doi.org/10.1007/s11707-012-0347-6

Barker, D. M., Lawler, D. M., Knight, D. W., Morris, D. G., Davies, H. N. and Stewart, E. J., 2009. Longitudinal

distributions of river flood power: the combined automated flood, elevation and stream power (CAFES) methodology. *Earth Surface Processes and Landforms*, 34(2), 280–290. DOI: https://doi.org/10.1002/esp.1723

Bielski, C., López-Vázquez, C., Grohmann, C. H., Guth, P. L., Hawker, L., Gesch, D. and Strobl, P., 2024. Novel approach for ranking DEMs: Copernicus DEM improves one arc second open global topography. *IEEE Transactions on Geoscience and Remote Sensing*, 62, 1–22. DOI: https://doi.org/10.1109/TGRS.2024.3368015

Biswas, B., KS, V. and Ranjan, R., 2021. Landslide susceptibility mapping using integrated approach of multi-criteria and geospatial techniques at Nilgiris district of India. *Arabian Journal of Geosciences*, 14(11), 980. DOI: https://doi.org/10.1007/s12517-021-07341-7

Bordoloi, A., Singh, K. K. and Gaichunglu, G., 2023. Application of analytical hierarchy process and GIS techniques to delineate the groundwater potential zones in and around Jorhat and Majuli areas of eastern Assam, India. *Model Earth Systems and Environment*, 9, 1589–1612. DOI: https://doi.org/10.1007/s40808-022-01583-4

Botzen, W. J. W., Aerts, J. C. J. H. and van den Bergh, J. C. J. M., 2012. Individual preferences for reducing flood risk to near zero through elevation. *Mitigation and Adaptation Strategies for Global Change*, (2), 229–244. DOI: https://doi.org/10.1007/s11027-012-9359-5

Bridge, J. S., 2009. Rivers and Floodplains: Forms, Processes and Sedimentary Record. John Wiley and Sons.

Cao, C., Xu, P., Wang, Y., Chen, J., Zheng, L. and Niu, C., 2016. Flash flood hazard susceptibility mapping using frequency ratio and statistical index methods in coalmine subsidence areas. *Sustainability*, 8(9), 948. DOI: https://doi.org/10.3390/su8090948

Cetin, M., Adiguzel, F. and Kaya, O., 2018. Mapping of bioclimatic comfort for potential planning using GIS in Aydin. *Environment, Development and Sustainability*, 20, 361–375. DOI: https://doi.org/10.1007/s10668-016-9885-5

Cetin, M., Zeren, I., Sevik, H., Cakir, C. and Akpinar, H., 2018. A study on the determination of the natural park's sustainable tourism potential. *Environmental Monitoring and Assessment*, 190(3), 167. DOI: https://doi.org/10.1007/s10661-018-6534-5

Chattaraj, D., Paul, B. and Sarkar, S., 2021. Integrated multi-parametric analytic hierarchy process (AHP) and geographic information system (GIS) based spatial modelling for flood and water logging susceptibility mapping: A case study of English Bazar Municipality of Malda, West Bengal, India. *Natural Hazards and Earth System Sciences Discussions*, 1–20. DOI: https://doi.org/10.5194/nhess-2020-399

Chen, W., Panahi, M. and Pourghasemi, H. R., 2017. Performance evaluation of GIS-based new ensemble data mining techniques of adaptive neuro-fuzzy inference system (ANFIS) with genetic algorithm (GA), differential evolution (DE) and particle swarm optimization (PSO) for landslide spatial modelling. *Catena*, 157, 310–324. DOI: https://doi.org/10.1016/j.catena.2017.05.034

Chen, W., Pourghasemi, H. R., Kornejady, A. and Zhang, N., 2017. Landslide spatial modeling: Introducing new ensembles of ANN, MaxEnt and SVM machine learning techniques. *Geoderma*, 305, 314–327. DOI: https://doi.org/10.1016/j.geoderma.2017.06.020

Costache, R. and Bui, D. T., 2019. Spatial prediction of flood potential using new ensembles of bivariate statistics and artificial intelligence: A case study at the Putna river catchment of Romania. *Science of The Total Environment*, 691, 1098–1118. DOI: https://doi.org/10.1016/j.scitotenv.2019.07.197

Costache, R., Pham, Q. B., Avand, M., Linh, N. T. T., Vojtek, M., Vojteková, J. and Dung, T. D., 2020. Novel hybrid models between bivariate statistics, artificial neural networks and boosting algorithms for flood susceptibility assessment. *Journal of Environmental Management*, 265, 110485. DOI: https://doi.org/10.1016/j.jenvman.2020.110485

Das, S. and Scaringi, G., 2021. River flooding in a changing climate: rainfall-discharge trends, controlling factors and susceptibility mapping for the Mahi catchment, Western India. *Natural Hazards*, 109, 2439–2459. DOI: https://doi.org/10.1007/s11069-021-04927-y

Das, S., 2018. Geographic information system and AHP-based flood hazard zonation of Vaitarna basin, Maharashtra, India. *Arabian Journal of Geosciences*, 11, 576. DOI: https://doi.org/10.1007/s12517-018-3933-4

Das, S., 2019. Comparison among influencing factor, frequency ratio and analytical hierarchy approach process techniques for groundwater potential zonation in Vaitarna basin, Maharashtra, India. *Groundwater for Sustainable Development*, 8, 617–629. DOI: https://doi.org/10.1016/j.gsd.2019.03.003

Das, S., 2019. Geospatial mapping of flood susceptibility and hydro-geomorphic response to the floods in Ulhas basin, India. *Remote Sensing Applications: Society and Environment*, 14, 60–74. DOI: https://doi.org/10.1016/j.rsase.2019.02.006

Das, S., Gupta, A. and Ghosh, S., 2017. Exploring groundwater potential zones using MIF techniques in semi-arid region: a case study of Hingoli district, Maharashtra. *Spatial Information Research*, 25(6), 749–756. DOI: https://doi.org/10.1007/s41324-017-0144-0

Das, S., Pardeshi, S. D., Kulkarni, P. P. and Doke, A., 2018. Extraction of lineaments from different azimuth angles using geospatial techniques: A case study of Pravara basin, Maharashtra, India. *Arabian Journal of Geosciences*, 11, 160. DOI: https://doi.org/10.1007/s12517-018-3522-6

Debnath, J., Sahariah, D., Mazumdar, M., et al., 2023. Evaluating Flood Susceptibility in the Brahmaputra River Basin: An Insight into Asia's Eastern Himalayan Floodplains Using Machine Learning and Multi-Criteria Decision-Making. *Earth System and Environment*, 7, 733–760. DOI: https://doi.org/10.1007/s41748-023-00358-w

Dejen, A. and Soni, S., 2021. Flash flood risk assessment using geospatial technology in Shewa Robit town, Ethiopia. *Model Earth Systems and Environment*, 7, 2599–2617. DOI: https://doi.org/10.1007/s40808-020-01016-0

Dhumal, H. T., Thakare, S. B., Londhe, S. and Rankhambe, P., 2022. Effect of flood releases from reservoirs in Krishna basin of Maharashtra state. *Innovative Infrastructure Solutions*, 7(1), 80. DOI: https://doi.org/10.1007/s41062-021-00678-8

Díaz-Alcaide, S. and Martínez-Santos, P., 2019. Advances in groundwater potential mapping. *Hydrogeology Journal*, 27(7), 2307–2324. DOI: https://doi.org/10.1007/s10040-019-02001-3

Dimri, A. P., Thayyen, R. J., Kibler, K., Stanton, A., Jain, S. K., Tullos, D. and Singh, V. P., 2016. A review of atmospheric and land surface processes with emphasis on flood generation in the Southern Himalayan rivers. *Science of the Total Environment*, 556, 98–115. DOI: http://dx.doi.org/10.1016/j.scitotenv.2016.02.206

Doke, A. B., Zolekar, R. B., Patel, H. and Das, S., 2021. Geospatial mapping of groundwater potential zones using multi-criteria decision-making AHP approach in a hardrock basaltic terrain in India. *Ecological Indicators*, 127, 107685. DOI: https://doi.org/10.1016/j.ecolind.2021.107685

Dottori, F.; Salamon, P.; Bianchi, Al.; Alfieri, L.; Hirpa, F. A. and Feyen, L., 2016. Development and evaluation of a framework for global flood hazard mapping. *Advances in Water Resources*, 94(), 87–102. DOI: https://doi.org/10.1016/j.advwatres.2016.05.002

Dou, X., Song, J., Wang, L., Tang, B., Xu, S., Kong, F. and Jiang, X., 2017. Flood risk assessment and mapping based on a modified multi-parameter flood hazard index model in the Guanzhong Urban Area, China. *Stochastic Environmental Research and Risk Assessment*, 32, 1131–1146. DOI: https://doi.org/10.1007/s00477-017-1429-5

Efraimidou, E. and Spiliotis, M., 2024. A GIS-Based Flood Risk Assessment Using the Decision-Making Trial and Evaluation Laboratory Approach at a Regional Scale. *Environmental Processes*, 11, (9). DOI: https://doi.org/10.1007/s40710-024-00683-w

Ekmekcioglu, O., Koc, K. and Ozger, M., 2021. District based flood risk assessment in Istanbul using fuzzy analytical hierarchy process. *Stochastic Environmental Research and Risk Assessment*, 35, 617–637. DOI: https://doi.org/10.1007/s00477-020-01924-8

Ekmekcioglu, O., Koc, K., Ozger, M., 2022. Towards flood risk mapping based on multi-tiered decision making in a densely urbanized metropolitan city of Istanbul. *Sustainable Cities and Society*, 80(2), 103759. DOI: https://doi.org/10.1016/j.scs.2022.103759

Elkhrachy, I., 2015. Flash flood hazard mapping using satellite images and GIS tools: A case study of Najran City, Kingdom of Saudi Arabia (KSA). *The Egyptian Journal of Remote Sensing and Space Science*, 18(2), 261-278. DOI: https://doi.org/10.1016/j.ejrs.2015.06.007

Farr, T. G., Rosen, P. A., Caro, E., Crippen, R., Duren, R., Hensley, S. and Alsdorf, D., 2007. The shuttle radar topography mission. *Reviews of Geophysics*, 45(2). DOI: https://doi.org/10.1029/2005RG000183

Fernández, D. S. and Lutz, M. A., 2010. Urban flood hazard zoning in Tucumán Province, Argentina, using GIS and multicriteria decision analysis. *Engineering Geology*, 111(1–4), 90–98. DOI: https://doi.org/10.1016/j.enggeo.2009.12.006

Forman, E. H., 1993. Facts and fictions about the analytic hierarchy process. *Mathematical and Computer Modelling*, 17(4–5), 19–26. DOI: https://doi.org/10.1016/0895-7177(93)90172-U

Fuller, I. C., 2008. Geomorphic impacts of a 100-year flood: Kiwitea Stream, Manawatu catchment, New Zealand. *Geomorphology*, 98(1–2), 84–95. DOI: https://doi.org/10.1016/j.geomorph.2007.02.026

Gaikwad, V. P., 2019. Assessment of morphometric characteristics and demarcation of ground water potential zones using geo spatial technique for vel and sal watershed, India. Unpublished M.Sc. thesis, Department of Geography, Savitribai Phule Pune University.

Gaikwad, V., Salunke, V., Jadhav, A. and Kudnar, N., 2024. Morphometric and longitudinal profile analysis in the Cauvery River basin: a geospatial approach. Arabian *Journal of Geosciences*, 17(10), 279. DOI: https://doi.org/10.1007/s12517-024-12079-z

Gaikwad, V., Singh, K., Salunke, V. and Kudnar, N., 2023. GIS-based comparative analysis of lineament extraction by using different azimuth angles: A case study of Mula river basin, Maharashtra, India. *Arabian Journal of Geosciences*, 16(9), 538. DOI: https://doi.org/10.1007/s12517-023-11636-2

Gangani, P., Mangukiya, N. K., Mehta, D. J., Muttil, N. and Rathnayake, U., 2023. Evaluating the efficacy of different DEMs for application in flood frequency and risk mapping of the Indian Coastal River Basin. *Climate*, 11(5), 114. DOI: https://doi.org/10.3390/cli11050114

Gigovic, L., Pamucar, D., Bajic, Z. and Drobnjak, S., 2017. Application of GIS-Interval Rough AHP Methodology for Flood Hazard Mapping in Urban Areas. *Water*, 9(6), 360. DOI: https://doi.org/10.3390/w9060360

Gokceoglu, C., Sonmez, H., Nefeslioglu, H. A., Duman, T. Y. and Can, T., 2005. The 17 March 2005 Kuzulu landslide (Sivas, Turkey) and landslide susceptibility map of its near vicinity. *Engineering Geology*, 81, 65–83. DOI: https://doi.org/10.1016/j.enggeo.2005.07.011

Grover, A., Saini, P. and Mahmood, G., 2024. Analysis of deccan trap area with special reference to hydro-landscape. *International Journal of Scientific Research and Engineering Development*, 5(6), 326-332, ISSN: 2581 - 717. DOI: https://doi.org/10.5281/zenodo.10465190

GSI [Geological Survey of India]. Geoscientific data of the Geological Survey of India.

Gupta, L. and Dixit, J., 2022. A GIS-based flood risk mapping of Assam, India, using the MCDA-AHP approach at the regional and administrative level. *Geocarto International*, 37(26), 11867–11899. DOI: https://doi.org/10.1080/10106049.2022.2060329

Halgamuge, M. N. and Nirmalathas, A., 2017. Analysis of large flood events: Based on flood data during 1985–2016 in Australia and India. *International Journal of Disaster Risk Reduction*, 24, 1–11. DOI: https://doi.org/10.1016/j.ijdrr.2017.05.011

Hammami, S., Dlala, M., Zouhri, L., et al., 2019. Application of the GIS based multi-criteria decision analysis and analytical hierarchy process (AHP) in the flood susceptibility mapping (Tunisia). *Arabian Journal of Geosciences*, 12, 1–16. DOI: https://doi.org/10.1007/s12517-019-4754-9

Ho-Hagemann, H. T. M., Hagemann, S. and Rockel, B., 2015. On the role of soil moisture in the generation of heavy rainfall during the Oder flood event in July 1997. *Tellus A: Dynamic Meteorology and Oceanography*, 67(1), 28661. DOI: https://doi.org/10.3402/tellusa.v67.28661

Hong, H., Tsangaratos, P., Ilia, I., Liu, J., Zhu, A.-X. and Chen, W., 2018. Application of fuzzy weight of evidence and data mining techniques in construction of flood susceptibility map of Poyang County, China. *Science of The Total Environment*, 625, 575–588. DOI: https://doi.org/10.1016/j.scitotenv.2017.12.256

Islam, A. R. M. T., Talukdar, S., Mahato, S., Kundu, S., Eibek, K. U., Pham, Q. B. and Linh, N. T. T., 2021. Flood susceptibility modelling using advanced ensemble machine learning models. *Geoscience Frontiers*, 12(3), 101075. DOI: https://doi.org/10.1016/j.gsf.2020.09.006

Islam, K., 2024. GIS based flood susceptibility mapping in the Keleghai river basin, India: A comparative assessment of bivariate statistical models. *Discover Water*, 4(1), 129. DOI: https://doi.org/10.1007/s43832-024-00186-7

Jain, S. K., Agarwal, P. K. and Singh, V. P., 2007. *Hydrology and Water Resources of India* (57). *Springer Science and Business Media*. DOI: https://doi.org/10.1007/1-4020-5180-8

Jebur, M. N., Pradhan, B. and Tehrany, M. S., 2014. Optimization of landslide causative factors using very

high-resolution airborne laser scanning (LiDAR) data at catchment scale. *Remote Sensing of Environment*, 152, 150–165. DOI: https://doi.org/10.1016/j.rse.2014.05.013

Jerin Joe, R. J., Pitchaimani, V. S., Kaliraj, S., Abishek, S. R., Promilton, A. A. A. and Karuppannan, S., 2025. Spatial modelling of groundwater potential zones in the Neyyar Basin using machine learning and morphometric analysis. *Scientific Reports*, 15(1), 36171. DOI: https://doi.org/10.1038/s41598-025-20000-1

Jonkman, S. N., 2005. Global perspectives on loss of human life caused by floods. *Natural Hazards*, 34(2), 151–175. DOI: https://doi.org/10.1007/s11069-004-8891-3

Kale, V. S. and Rajaguru, S. N., 1987. Late Quaternary alluvial history of the northwestern Deccan upland region. *Nature*, 325(6105), 612–614. DOI: https://doi.org/10.1038/325612a0

Kalita, N., Bora, A. K., Sarmah, R., Sahariah, D. and Nath, M. J., 2025. Comparative Flood Hazard Assessment in Assam's Belsiri River Basin Using AHP and MaxEnt Models. *Revue Internationale de Géomatique*, 34. DOI: https://doi.org/10.32604/rig.2024.058265

Kaur, H., Gupta, S. and Parkash, S., 2017. Geospatial modelling of flood susceptibility pattern in a subtropical area of West Bengal, India. *Environmental Earth Sciences*, 76, 339. DOI: https://doi.org/10.1007/s12665-017-6667-9

Kayastha, P., Dhital, M. R. and De Smedt, F., 2013. Application of the analytical hierarchy process (AHP) for landslide susceptibility mapping: A case study from the Tinau watershed, west Nepal. *Computers and Geosciences*, 52, 398–408. DOI: https://doi.org/10.1016/j.cageo.2012.11.003

Kazakis, N., Kougias, I. and Patsialis, T., 2015. Assessment of flood hazard areas at a regional scale using an index-based approach and analytical hierarchy process: application in Rhodope-Evros region, Greece. *Science of The Total Environment*, 538, 555–563. DOI: https://doi.org/10.1016/j.scitotenv.2015.08.055

Khodaei, H., Nasiri Saleh, F., Nobakht Dalir, A. and Zarei, E., 2025. Future flood susceptibility mapping under climate and land use change. *Scientific Reports*, 15(1), 12394. DOI: https://doi.org/10.1038/s41598-025-97008-0

Khosravi, K., Pourghasemi, H. R., Chapi, K. and Masoumeh, B., 2016. Flash flood susceptibility analysis and its mapping using different bivariate models in Iran: A comparison between Shannon's entropy, statistical index and weighting factor models. *Environmental Monitoring and Assessment*, 188, 656. DOI: https://doi.org/10.1007/s10661-016-5665-9

Khosravi, K., Shahabi, H., Pham, B. T., Adamowski, J., Shirzadi, A., Pradhan, B. and Prakash, I., 2019. A comparative assessment of flood susceptibility modeling using multi-criteria decision-making analysis and machine learning methods. *Journal of Hydrology*, 573, 311–323. DOI: https://doi.org/10.1016/j.jhydrol.2019.03.073

Kim, B. and Kim, H., 2014. Evaluation of flash flood severity in Korea using the modified flash flood index (MFFI). *Journal of Flood Risk Management*, 7, 344–356. DOI: https://doi.org/10.1111/jfr3.12057

Knighton, A. D., 1999. Downstream variation in stream power. *Geomorphology*, 29(3–4), 293–306. DOI: https://doi.org/10.1016/S0169-555X(99)00015-X

Knighton, D., 2014. *Fluvial Forms and Processes: A New Perspective*. Routledge. DOI: https://doi.org/10.4324/9780203784662

Kourgialas, N. N. and George P. Karatzas, 2011. Flood management and a GIS modelling method to assess flood-hazard areas—a case study. *Hydrological Sciences Journal*, 56:2, 212–225. DOI: https://doi.org/10.1080/02626667.2011.555836

Krishna River Basin Report, Central Water Commission (CWC) and National Remote Sensing Centre (NRSC), Indian Space Research Organisation (ISRO), 2014. Government of India Report (2.0), 1–180.

Krishnan, A., Dev, S. D., Arjun, S., Deepchand, V., Singh, Y., Shaji, E. and Krishnaprasad, P. K., 2025. Flood susceptibility mapping in Kali River Basin, Southern India: A GIS-based analytical hierarchy process modelling. *Results in Earth Sciences*, 3, 100079. DOI: https://doi.org/10.1016/j.rines.2025.100079

Kumar, A. U. and Jayakumar, K. V., 2020. Hydrological alterations due to anthropogenic activities in Krishna River Basin, India. *Ecological Indicators*, 108, 105663. DOI: https://doi.org/10.1016/j.ecolind.2019.105663

Kvocka, D., Falconer, R. A. and Bray, M., 2016. Flood hazard assessment for extreme flood events. *Natural Hazards*, 84, 1569–1599. DOI: https://doi.org/10.1007/s11069-016-2501-z

Leopold, L. B. and Wolman, M. G., 1970. River channel patterns. In Rivers and River Terraces (pp. 197–237). *Palgrave Macmillan UK*. DOI: https://doi.org/10.1007/978-1-349-15382-4_8

Lim, J. and Lee, K. S., 2017. Investigating flood susceptible areas in inaccessible regions using remote sensing and geographic information systems. *Environmental Monitoring And Assessment*, 189(3), 96. DOI: https://doi.org/10.1007/s10661-017-5811-z

Mahmoud, S. H. and Gan, T. Y., 2018. Multi-criteria approach to develop flood susceptibility maps in arid regions of Middle East. *Journal of Cleaner Production*, 196, 216–229. DOI: https://doi.org/10.1016/j.jclepro.2018.06.047

Maity, D. K. and Mandal, S., 2019. Identification of groundwater potential zones of the Kumari river basin, India: An RS and GIS based semi-quantitative approach. *Environment, Development and Sustainability*, 21, 1013–1034. DOI: https://doi.org/10.1007/s10668-017-0072-0

Malekian, A. and Azarnivand, A., 2016. Application of Integrated Shannon's Entropy and VIKOR techniques in prioritization of food risk in the Shemshak watershed. *Iran Water Resources Management*, 30(1), 409–425. DOI: https://doi.org/10.1007/s11269-015-1169-6

Marvi, M. T., 2020. A review of flood damage analysis for a building structure and contents. *Natural Hazards*, 102, 967–995. DOI: https://doi.org/10.1007/s11069-020-03941-w

Memon, A., Shah, N., Thakkar, D. and Patel, Y., 2025. Statistical evaluation of open source DEMs for accurate watershed delineation in sustainable river basin management. *Discover Geoscience*, 3(1), 151. DOI: https://doi.org/10.1007/s44288-025-00276-6

Merkuryeva, G., Merkuryev, Y., Sokolov, B. V., Potryasaev, S., Zelentsov, V. A. and Lektauers, A., 2015. Advanced river flood monitoring, modelling and forecasting. *Journal of Computational Science*, 10, 77–85. DOI: https://doi.org/10.1016/j.jocs.2014.10.004

Merz, B., Thieken, A. H. and Gocht, M., 2007. Flood risk mapping at the local scale: concepts and challenges. In Flood Risk Management in Europe: Innovation in Policy and Practice (231–251). *Springer Netherlands*. DOI: https://doi.org/10.1007/978-1-4020-4200-3

Meshram, S. G., Alvandi, E. and Singh, V. P., 2019. Comparison of AHP and fuzzy AHP models for prioritization of watersheds. *Soft Computing*, 23, 13615–

13625. DOI: https://doi.org/10.1007/s00500-019-03900-z

Miguez, M. G. and de Magalhaes, L. P. C., 2010. Urban flood control, simulation and management–an integrated approach. *In Methods and Techniques in Urban Engineering* (131–160).

Mojaddadi, H., Pradhan, B., Nampak, H., Ahmad, N. and Ghazali, A. H. bin., 2017. Ensemble machine-learning-based geospatial approach for flood risk assessment using multi-sensor remote-sensing data and GIS. *Geomatics, Natural Hazards and Risk*, 8(2), 1080–1102. DOI: https://doi.org/10.1080/19475705.2017.1294113

Moore, I. D., Grayson, R. B. and Ladson, A. R., 1991. Digital terrain modelling: A review of hydrological, geomorphological and biological applications. *Hydrological Processes*, 5(1), 3–30. DOI: https://doi.org/10.1002/hyp.3360050103

Muis, S., Guneralp, B., Jongman, B., Aerts, J. C. and Ward, P. J., 2015. Flood risk and adaptation strategies under climate change and urban expansion: A probabilistic analysis using global data. *Science of The Total Environment*, 538, 445–457. DOI: http://dx.doi.org/10.1016/j.scitotenv.2015.08.068

Murmu, P., Kumar, M., Lal, D., Sonker, I. and Singh, S. K., 2019. Delineation of groundwater potential zones using geospatial techniques and analytical hierarchy Process in Dumka District, Jharkhand, India. *Groundwater for Sustainable Development*, 9, 100239. DOI: https://doi.org/10.1016/j.gsd.2019.100239

Navale, S. and Bhagat, V., 2021. Detection and delineation of potential areas for tourism activities in coastal zone of Ratnagiri district, Maharashtra (India). Journal *Geographical Studies*, 5(2), 79–113. DOI: https://doi.org/10.21523/gcj5.21050203

NBSS and LUP [National Bureau of Soil Survey and Land Use Planning]. Indian Council of Agricultural Research, Department of Agricultural Research and Education, Ministry of Agriculture, Government of India.

Nguyen, H. N., Fukuda, H. and Nguyen, M. N., 2024. Assessment of the susceptibility of urban flooding using GIS with an analytical hierarchy process in Hanoi, Vietnam. *Sustainability*, 16(10), 3934. DOI: https://doi.org/10.3390/su16103934

NRSC [National Remote Sensing Centre]. Bhuvan Geo Portal and Web Services Group (BGWSG), National Remote Sensing Centre, Indian Space Research Organisation (ISRO), Government of India.

Olii, M. R., Olii, A. and Pakaya, R., 2021. The integrated spatial assessment of the flood hazard using AHP-GIS: The case study of Gorontalo Regency. *Indonesian Journal of Geography*, 53(1). DOI: https://doi.org/10.22146/ijg.59999

Paswan, A., Agarwal, A., Kumar, V. and Varma, S., 2025. Multicriteria decision-making for sustainable groundwater in Deccan Plateau basalts. *Journal of Hydrology: Regional Studies*, 51, 101–110. DOI: https://doi.org/10.1016/j.gsd.2025.101511

Patil, A. S., Teli, S. S., Drakshe, P. P., Patil, P. A., Kadam, A. D., Powar, G. P. and Panhalkar, S. S., 2024. Comparative analysis of machine learning, statistical and MCDA methods for rainfall-induced landslide susceptibility mapping in the eco-sensitive Koyna River basin of India. *Indian Geotechnical Journal*, 1–26. DOI: https://doi.org/10.1007/s40098-024-00957-y

Pawluszek, K. and Borkowski, A., 2017. Impact of DEM-derived factors and analytical hierarchy process on landslide susceptibility mapping in the region of Rożnów Lake, Poland. *Natural Hazards*, 86, 919–952. DOI: https://doi.org/10.1007/s11069-016-2725-y

Pham, B. T., Avand, M., Janizadeh, S., Phong, T. V., Al-Ansari, N., Ho, L. S., Das, S., Le, H. V., Amini, A., Bozchaloei, S. K., Jafari, F. and Prakash, I., 2020. GIS based hybrid computational approaches for flash flood susceptibility assessment. *Water*, 12(3), 683. DOI: https://doi.org/10.3390/w12030683

Pourzangbar, A., Oberle, P., Kron, A. and Franca, M. J., 2025. Analysis of the utilization of machine learning to map flood susceptibility. *Journal of Flood Risk Management*, 18(2), e70042. DOI: https://doi.org/10.1111/jfr3.70042

Razavi-Termeh, S. V., Sadeghi-Niaraki, A., Jelokhani-Niaraki, M. and Choi, S. M., 2025. Flood susceptibility mapping using optimized deep learning models: A non-structural framework. *Applied Water Science*, 15(8), 1–25. DOI: https://doi.org/10.1007/s13201-025-02548-5

Risi, R. D., Jalayer, F., Paola, F. D. and Lindley, S., 2017. Delineation of flooding risk hotspot based on digital elevation model, calculated and historical flooding extents: The case of Ouagadougou. *Stochastic Environmental Research and Risk Assessment*, 32, 1545–1559. DOI: https://doi.org/10.1007/s00477-017-1450-8

Rojas, R., Feyen, L., Bianchi, A. and Dosio, A., 2012. Assessment of future flood hazard in Europe using a large ensemble of bias-corrected regional climate simulations. *Journal of Geophysical Research: Atmospheres*, 117, D17109. DOI: https://doi.org/10.1029/2012JD017461

Saaty, T. L., 1977. A scaling method for priorities in hierarchical structures. *Journal of Mathematical Psychology*, 15(3), 234–281. DOI: https://doi.org/10.1016/0022-2496(77)90033-5

Saaty, T. L., 1983. Priority setting in complex problems. *IEEE Transactions on Engineering Management*, 30(3), 140–155. DOI: https://doi.org/10.1109/TEM.1983.6448606

Saha, A. K. and Agrawal, S., 2020. Mapping and assessment of flood risk in Prayagraj district, India: A GIS and remote sensing study. *Nanotechnology for Environmental Engineering*, 5(2), 11. DOI: https://doi.org/10.1007/s41204-020-00073-1

Schauble, H., Marinoni, O. and Hinderer, M., 2008. A GIS-based method to calculate flow accumulation by considering dams and their specific operation time. *Computers and Geosciences*, 34(6), 635–646. DOI: https://doi.org/10.1016/j.cageo.2007.05.023

Shekhar, S. and Pandey, A. C., 2014. Delineation of groundwater potential zone in hard rock terrain of India using remote sensing, geographical information system (GIS) and analytic hierarchy process (AHP) techniques. Geocarto *International*, 30(4), 402–421. DOI: https://doi.org/10.1080/10106049.2014.894584

Su, W., Zhang, X., Wang, Z., Su, X., Huang, J., Yang, S. and Liu, S., 2011. Analyzing disaster-forming environments and the spatial distribution of flood disasters and snow disasters that occurred in China from 1949 to 2000. *Mathematical and Computer Modelling*, 54(3–4), 1069–1078. DOI: https://doi.org/10.1016/j.mcm.2010.11.037

Subbarayan, S. and Sivaranjani, S., 2020. Modelling of flood susceptibility based on GIS and analytical hierarchy process- A case study of Adayar River Basin. Tamilnadu, India. *An Interdisciplinary Approach for Disaster Resilience and Sustainability*, 91–110. DOI: https://doi.org/10.1007/978-981-32-9527-8_6

Subramanian, V., 1993. Sediment load of Indian rivers. *Current Science*, 928–930.

Suykens, C., Priest, S. J., van Doorn-Hoekveld, W. J., Thuillier, T. and van Rijswick, M., 2016. Dealing with flood

damages: Will prevention, mitigation and ex post compensation provide for a resilient triangle? *Ecology and Society*, 21(4), 1. DOI: http://dx.doi.org/10.5751/ES-08592-210401

Tehrany, M. S., Pradhan, B. and Jebur, M. N., 2013. Spatial prediction of flood susceptible areas using rule based decision tree (DT) and a novel ensemble bivariate and multivariate statistical models in GIS. *Journal of Hydrology*, 504, 69–79. DOI: http://dx.doi.org/10.1016/j.jhydrol.2013.09.034

Tehrany, M. S., Pradhan, B. and Jebur, M. N., 2014. Flood susceptibility mapping using a novel ensemble weights-of-evidence and support vector machine models in GIS. *Journal of Hydrology*, 512, 332–343. DOI: https://doi.org/10.1016/j.jhydrol.2014.03.008

Tehrany, M. S., Pradhan, B. and Jebur, M. N., 2015. Flood susceptibility analysis and its verification using a novel ensemble support vector machine and frequency ratio method. *Stochastic Environmental Research and Risk Assessment*, 29(4), 1149–1165. DOI: https://doi.org/10.1007/s00477-015-1021-9

Tehrany, M. S., Pradhan, B., Mansor, S. and Ahmad, N., 2015. Flood susceptibility assessment using GIS-based support vector machine model with different kernel types. *Catena*, 125, 91–101. DOI: https://doi.org/10.1016/j.catena.2014.10.017

Tepetidis, N., Benekos, I., Iliopoulou, T., Dimitriadis, P. and Koutsoyiannis, D., 2025. Combining machine learning models and satellite data of an extreme flood event for flood susceptibility mapping. *Water*, 17(18), 2678. DOI: https://doi.org/10.3390/w17182678

Terker, P. U., 2024. Stratigraphy, composition and form of Deccan basalt lava flows in Aurangabad and Ahmednagar districts. *International Journal of Geography, Geology and Environment*, 7(5), 35–46.

Tique, W. F. M., Sapena, M., Weigand, M., Groth, S., Geiß, C. and Taubenböck, H., 2025. *A comparative assessment of data-driven flood susceptibility mapping in Nigeria. Preprint.* DOI: https://doi.org/10.21203/rs.3.rs-6756403/v1

TOI [Times of India], 2024. The Times of India.

Tran, C. K., Dang, N. D., Nguyen, D. M., Nguyen, B. T. N., Le, B. T. H., Vo, H. C. and La, H. P., 2025. Real-time flood forecasting using time-varying parameter hydrological model: Case study for Ta Trach reservoir. *Applied Water Science*, 15(7), 1–13. DOI: https://doi.org/10.1007/s13201-025-02503-4

Vojtek, M. and Vojtekova, J., 2016. Flood hazard and flood risk assessment at the local spatial scale: a case study. *Geomatics, Natural Hazards and Risk*, 7(6), 1973–1992. DOI: https://doi.org/10.1080/19475705.2016.1166874

Wale, P. B., Sivasankar, T., Sanyal, R., Ghosh, S. and Srivastava, H., 2025. Flood susceptibility assessment of Kaziranga National Park using ensemble machine learning algorithms and Sentinel-1 SAR data. *Journal of the Indian Society of Remote Sensing*. DOI: https://doi.org/10.1007/s12524-025-02320-x

Wang, L., Cui, S., Li, Y., Huang, H., Manandhar, B., Nitivattananon, V., Fang, X. and Huang, W., 2022. A review of the flood management: From flood control to flood resilience. *Heliyon*, 8(11). DOI: https://doi.org/10.1016/j.heliyon.2022.e11763

Ward, R. C. and Robinson, M., 1975. *Principles of Hydrology* (367). McGraw-Hill.

Winsemius, H., Aerts, J., van Beek, L., et al., 2016. Global drivers of future river flood risk. *Nature Climate Change*, 6, 381–385. DOI: https://doi.org/10.1038/nclimate2893

WRIS [Water Resource Information System], 2018. Department of Water Resources, Ministry of Jal Shakti, Government of India.

Yilmaz, O. S., 2022. Flood hazard susceptibility areas mapping using Analytical Hierarchical Process (AHP), Frequency Ratio (FR) and AHP-FR ensemble based on Geographic Information Systems (GIS): a case study for Kastamonu, Türkiye. *Acta Geophysica*, 70(6), 2747–2769. DOI: https://doi.org/10.1007/s11600-022-00882-9

Yong, B., Ren, L. L., Hong, Y., Gourley, J. J., Chen, X., Zhang, Y. J. and Wang, W. G., 2012. A novel multiple flow direction algorithm for computing the topographic wetness index. *Hydrology Research*, 43(1–2), 135–145. DOI: https://doi.org/10.2166/nh.2011.115

Yu, Q., Wang, Y. and Li, N., 2022. Extreme flood disasters: Comprehensive impact and assessment. *Water*, 14(8), 1211. DOI: https://doi.org/10.3390/w14081211

Zhang, N. and Alipour, A., 2021. A multi-step assessment framework for optimization of flood mitigation strategies in transportation networks. *International Journal of Disaster Risk Reduction*, 63, 102439. DOI: https://doi.org/10.1016/j.ijdrr.2021.102439

Zhran, M., Ghanem, K., Tariq, A., Alshehri, F., Jin, S., Das, J. and Mousa, A., 2024. Exploring a GIS-based analytic hierarchy process for spatial flood risk assessment in Egypt: A case study of the Damietta branch. *Environmental Sciences Europe*, 36(1), 184. DOI: https://doi.org/10.1186/s12302-024-01001-9

*****